Hydrogen in Metals - A Nondestructive Test

by

Thomas S. Lubnow, Jr.

thesis submitted to the Faculty of the

Virginia Polytechnic Institute and State University

in partial fulfillment of the requirements for the degree of

Master of Science

in

Materials Engineering

APPROVED:

M.R. Louthan, Jr., Chairman

Robert E. Swanson

J.C. Duke

July, 1986

Blacksburg, Virginia

Hydrogen in Metals - A Nondestructive Test

by

Thomas S. Lubnow, Jr.

M.R. Louthan, Jr., Chairman

Materials Engineering

(ABSTRACT)

In many manufacturing and service industries a need exists for a nondestructive test to determine the presence of hydrogen in a material system. The feasibility of such a system is examined here.

Acoustic emission activity resulting from a microhardness indentation is employed to detect hydrogen in A106 and 4340 steel bars following cathodic, gaseous, and chemical charging. These tests show a large increase in emission energy after charging followed by a drop to precharge levels with time. These activity levels are used to calculate hydrogen diffusivity and binding energy of hydrogen to traps in the steel. A mechanism of acoustic emission generation is proposed involving the breakaway of dislocations from Cottrell-like hydrogen atmospheres.

The effects of surface roughness and microstructure are also evaluated. Testing of various surfaces indicates that limited surface preparation is necessary prior to implementing the test procedure. Low activity levels before and after charging in 4340, and in martensitic and bainitic A106 indicate possible difficulties in applying the test to harder, more dispersed structures.

Despite this limitation and a large amount of scatter in the acquired data, the results indicate that acoustic emission monitoring of microhardness indentations may be of value in detecting the presence of hydrogen in metals and as a research tool in the study of hydrogen transport and embrittlement mechanisms.

Acknowledgements

The author would like to express deepest thanks to his advisor, M. R. Louthan, Jr. for all of his support over the last two years, and to Mrs. Louthan and Amy for being great friends and for putting up with the "mess downstairs".

Much thanks is also extended to Drs. J. C. Duke and Robert Swanson who went beyond the duties of committee members to give guidance throughout this investigation.

The author would also like to thank friends, roommates and coworkers for their help and support. In particular, Kevin, Paul, Dan, Neil and Sue for providing enough distractions to keep things interesting. Buddy Luken for his photography skills as well as for being a good friend and roommate. Mike Kiernan, for his help in understanding some of the subtleties of acoustic emission. Kathy Rohr for exposing the author to the diligent, organized approach to graduate studies and Danny Harvey and Bill Porr who at least approached if not exceeded the author's nonchalant attitude. Pat Simmons, whose assistance in every aspect of this investigation, thought provoking discussions and enthusiasm made this work possible. Karen Snider, Jeanne Warner, Ann Rogers, and Kim Kessinger whose fantastic personalities and amazing ability to keep the department running smoothly, made going upstairs a pleasure.

Finally, the author would like to thank his parents, Thomas and Patricia for all of their guidance and encouragement over the years.

Table of Contents

List of Illustrations

List of Tables

1.0 Introduction

The deleterious effects of hydrogen on the mechanical properties of material systems have been well documented. Embrittlement resulting from in-service exposure to gaseous hydrogen and to hydrogen evolved from corrosion processes has frequently resulted in costly catastrophic failure. Various manufacturing and fabrication processes can also result in hydrogen uptake. Such processes include melting and casting, pickling, welding, and electroplating. Hydrogen uptake during plating operations can be especially damaging because hydrogen desorption may be inhibited by the barrier formed by the applied coating. Thus, hydrogen adsorbed during the processing of the component will be retained and may severely affect performance when the material is later subjected to in-service loading.

To alleviate the problem of hydrogen uptake during plating components are frequently subjected to bake-out procedures following the plating process. Bakeout is performed by maintaining the component at a temperature of 150^{O}to 250^{O}C for a period of time sufficient to allow outgassing of hydrogen to subcritical levels. The consequences of insufficient bake-out times are obvious; however, the economic consequences of needlessly prolonged or unnecessary bake-out are also of major concern to manufacturers. Manufacturers would benefit greatly from a nondestructive test that could detect the presence of a critical hydrogen concentration. In addition to serving the plating industry, such a test could be used to monitor a wide variety of structures exposed to hydrogen.

These structures include gas storage and transport facilities, chemical plant components and various parts of conventional and nuclear power generating systems.

The primary purpose of this investigation was to determine the feasibility of developing such a test by combining two common nondestructive evaluation techniques, microhardness and acoustic emission. In addition, it was hoped that the studies would lead to new insights into hydrogen transport processes and mechanisms of hydrogen embrittlement.

2.0 Literature review

Electroplating is a common procedure in which a thin metal coating is deposited electrochemically on the surface of a component. Electroplating provides desirable corrosion protection at the surface while retaining favorable mechanical properties of the base metal.

However inherent to the plating process is the cathodic reaction: $H^+ + e^- \rightarrow H$. This evolved hydrogen is frequently then adsorbed by the metal. The plating will subsequently serve as a barrier to effusion of the hydrogen from the metal and hydrogen embrittlement may result (1,2,3).

A number of cases of hydrogen induced delayed failure associated with electroplating operations are discussed in Volume 10 of the ASM Metals Handbook. In particular, an example on page 480 begins:

> "cadmium plated high strength steel bolts were used to facilitate quick disassembly of a vehicle. One bolt was found fractured across the root of the thread after being torqued in place for one week ... It was assumed that the bolts had not been given a baking treatment for the removal of hydrogen. Because there is no nondestructive test to confirm such an assumption, two of the bolts were baked at 205 C for 24 hours, then a series of (destructive) tests were performed on both the baked and as plated bolts"

This example then concludes that the failure of the bolt was due to "time dependent hydrogen embrittlement" and states that "Baking for 1/2 hour is the minimum baking time; however, baking times of up to 24 hours are recommended for absolute safety." The preceding quote illustrates two

of the major problems which beset manufacturers who conduct electroplating. The primary one being hydrogen induced delayed failure. However, the significance of this problem has been greatly enhanced by the second problem, that of a lack of a nondestructive test to detect the presence of hydrogen in a component and to evaluate the effectiveness of bakeout procedures. Hydrogen embrittlement is by no means exclusively a result of electroplating. However, embrittlement due to electroplating is somewhat unique in that the hydrogen embrittlement problem can almost always be avoided through the adequate implementaion of bakeout procedures. The implementation of these bakeout procedures would surely be facilitated by a simple nondestructive test to evaluate their effectiveness. Such a test would therefore result in the prevention of a great number of unnecessary failures.

The following section is a general discussion of hydrogen embrittlement. This discussion is followed by two passages which briefly describe the two components of the proposed nondestructive test system, acoustic emission and microhardness indentation.

2.1 Hydrogen Effects

The effects of hydrogen on the behavior of various metals has been subject to much study over the past forty years. Despite the efforts of many investigators there has been little agreement on the basic mechanisms of hydrogen embrittlement. However, it has become very clear that the effects of hydrogen on the mechanical behavior of a given alloy are specific to that particular metal. These effects have been found to include decreased strain to fracture (4), change in fracture mode (5,6), and decreased fatigue life (7,8). Perhaps even more numerous than the effects of hydrogen are the experimental variables which have been found to influence the embrittlement process. Some of these factors are strain rate (9,10,12), stress state (9,10,11,25), temperature (12,16), hydrogen concentration (11,18), specimen geometry (11,17) and microstructure (13,14,20). This wide range of

test variables has contributed to the generation of many proposed mechanisms to explain the specific hydrogen effects seen in certain materials. Most of these mechanisms cannot be disproved in their application to the specific alloy and test procedure to which they were postulated. However, in attempting to broaden the scope of a particular mechanism, inevitably there exists substantial data to refute it. It is growing increasingly evident that the search for a "universal" hydrogen embrittlement theory may be futile because it is likely that a variety of mechanisms are contributing to the embrittlement process. The dominance of any one particular mechanism over another is highly dependent on the specific alloy and test conditions.

For the most part, the wide variety of proposed hydrogen embrittlement mechanisms can be broken down into two broad categories (15,31)

1. Hydrogen effects on lattice and interfacial cohesive strengths (24,26,27,41)

2. Hydrogen effects on dislocation motion

The interfacial strength models are based on a Griffith type analysis of brittle fracture (24). The Griffith analysis states that crack growth will occur when the strain energy released by a propagating crack is greater than the energy expended in the formation of new surface area. This analysis results in the familiar Griffith relation

$$\sigma_f \sim \left(\frac{E\gamma}{\pi a}\right)^{\frac{1}{2}} \qquad 2.1$$

These models propose that hydrogen lowers the surface energy, thereby reducing γ in Equation 2.1 and allowing crack propagation at low applied loads (27). It is widely accepted that hydrogen induced decreases in surface energy and interfacial cohesive strength contribute in at least some cases to hydrogen embrittlement. However, the lack of embrittlement from exposure to certain other environmental agents that are equal or greater in their surface wetting capacity (8,9,18) and evidence

of ductile fracture features in certain materials that have experienced "embrittlement", rule out this simple surface energy mechanism as a complete explanation for hydrogen embrittlement.

Many of the mechanisms that have proposed interfacial decohesion due to hydrogen are dependent on localization of large quantities of hydrogen at these interfaces (25,40). This localization of hydrogen in a system sometimes manifests itself in delayed failure. Delayed failure is an aspect of hydrogen embrittlement in which the interfacial decohesion mechanism is very much accepted and well characterized. This hydrogen effect commonly occurs when a component possessing some hydrogen concentration is subject to a sustained load. Therefore, this problem often occurs in electroplated components when hydrogen adsorbed during processing is retained and redistributed. Hydrogen transport by dislocation motion and by diffusion promote localization of very large hydrogen concentrations in areas of lattice dilation and in regions where dislocation motion is inhibited. Accumulation of hydrogen concentrations at grain boundaries, crack tips, and other microstructural discontinuities effectively reduces the strength of these interfaces promoting brittle failure (24,40). Therefore, the interaction of hydrogen with dislocations and resulting transport are important considerations with regard to interfacial fracture, embrittlement mechanisms.

More obvious perhaps is the importance of hydrogen/dislocation interactions on those mechanisms involving plastic flow. There exists wide disagreement on the hydrogen effects on plastic behavior. Various investigators have proposed that hydrogen decreases (22,24,30,18), increases (21,24), or has no effect on flow stress (6,18). There does exist universal agreement that dislocations represent favorable sites for hydrogen atoms. Along with this agreement there is a consensus that hydrogen can be transported by the motion of dislocations to which it is bound (12,32,39,40).

A number of investigators have proposed that along with this binding and transport, hydrogen enhances ductile processes (22,23,38). This argument is based primarily on irreversible thermodynamics considerations which imply that if dislocation motion will enhance hydrogen transport, greater hydrogen concentrations will neccessarily facilitate dislocation motion (29). This idea has contributed to the formulation of an embrittlement model based on enhanced ductility.

This model states that "embrittlement" occurs by an autocatalytic decrease in flow stress resulting from localization of large hydrogen concentrations by the enhanced dislocation motion (23). The enhanced ductility models have been substantiated by retained ductile features (microvoids) on fracture surfaces of supposedly embrittled samples (23,42) and through those reports which cite reduction in yield stress subsequent to hydrogen exposure.

However, the investigators which cite reductions in yield stress may be flawed by their failure to acknowledge the effects of internal pressures generated by high hydrogen concentration or reduction in effective cross sectional area due to minute surface cracks (18). This model also does not consider changes in fracture surface features from microvoid coalescence, which commonly occur. Based on these considerations it is perhaps more widely accepted that hydrogen will retard dislocation motion and thereby increase flow stress and strain hardening capacity (1,18,24). In order to more thoroughly consider the effects of hydrogen on flow, more discussion of the transport of hydrogen by dislocations is in order.

The binding energy for hydrogen to a dislocation is given by

$$u = \frac{A}{R} \sin\theta \qquad 2.2$$

where A is a constant related to the misfit strain around the dislocation and R is the distance from the dislocation core. The binding energy has been cited by numerous investigations and is generally accepted to be approximately 0.3 eV/atom at the core of the dislocation (44). The concentration at the dislocation is given then in terms of the bulk concentration (Co) as

$$C = C_o \exp(\frac{u}{RT}) \qquad 2.3$$

Equation 2.3 shows that at higher temperatures thermal activation of the dislocation and hydrogen atmosphere result in the dislocation no longer remaining a preferred site. Similarly, at high diffusivities and large lattice dilations resulting from hydrostatic tension the hydrogen affinity for the dislocation decreases. The influence of the hydrogen atmosphere on dislocation mobility is determined by this binding energy and is therefore also affected by temperature and stress state. The maximum possible influence exerted by the atmosphere occurs upon dislocation breakaway when the binding energy must be exceeded. If the dislocation is carrying the atmosphere directly, some energy value less than the binding energy is acting to retard dislocation mobility. Breakaway is clearly required for dislocation motion away from carbon atoms because of the low diffusivity of carbon in iron ($\sim 10^{-22}$ cm^2/s) (30). However, because of the high diffusivity of hydrogen the exact mechanism of hydrogen/dislocation interaction is not clear. The idea that a hydrogen atmosphere can effectively pin a dislocation was first proposed by Frank and has since seen substantial experimental justification (1,36,37,39,77). Serrated yielding has been noted following hydrogen exposure in a variety of alloys (36,37,39) thereby indicating that hydrogen can act as a pinning point and necessitate dislocation breakaway before flow can occur. Evidence of hydrogen influence on the onset of ductility has also been shown by hydrogen-induced anomalies in yield point behavior of A106 steel (30). The lack of a clear yield point in A106 after hydrogen exposure has been attributed to hydrogen atoms replacing carbon atoms as pinning points.

Aside from the simple drag of hydrogen on dislocations, there have been a number of other mechanism proposed by which hydrogen can retard ductile processes. Increased strain hardening rates after hydrogen exposure in a number of different alloys have been explained by the lowering of stacking fault energy by hydrogen (30). The lowering of stacking fault energy will decrease the ability of dislocations to cross-slip and will lead to dislocation multiplication. Increased dislocation density and lack of cross-slip ability will substantially increase work hardening rates (30).

However, the effect of hydrogen on the onset of flow, rather than strain hardening is most crucial in terms of embrittlement processes. The process of crack blunting, for example, is dependent on the initiation of ductile processes at the crack tip. It has been found that in a high strength steel

the fatigue life of samples with carefully polished surfaces is extended by the presence of hydrogen. However, if the surface is rough, fatigue life is diminished greatly. This phenomenon of extended life has been explained by the suppression by hydrogen of ductile processes which initiate fatigue cracks. If the starter sites are provided (by the surface roughness), hydrogen prohibits ductile processes which blunt cracks and life is shortened (33,35).

It is clear that no discussion of hydrogen embrittlement is complete without the consideration of hydrogen transport and the effects of hydrogen on local ductile processes. This report will attempt to use acoustic emission resulting from this highly localized plasticity to gain insight as to the manner and degree with which hydrogen is interacting with dislocations and then postulate how this interaction could affect the embrittlement process.

2.2 *Acoustic Emission Testing*

Acoustic emission (AE) is the detectable elastic energy which is released when materials undergo some form of deformation or fracture. Monitoring of these emissions has gained widespread application as a passive nondestructive test to evaluate structural integrity, to denote processes corresponding to the onset of catastrophic failure and as a research tool to analyze and develop models for the mechanisms involved in the failure of engineering materials and structures. The main advantage of AE analysis is that it is inherently sensitive to local, transient material instabilities (45). Almost without exception unstable conditions are generated locally long before failure occurs. These local instabilities occur as the material proceeds to a lower energy state and therefore release detectable elastic energy when they occur. These detectable AE events are often instrumental in the first stages of failure. Thus, through analysis of acoustic emission it is possible that one can develop a fundamental understanding of the failure process. Some typical emission generating events which precede failure are "ductile" processes like formation and propagation of slip bands, and other highly

localized dislocation motion or "brittle" processes, such as grain boundary reorientation, crack propagation and fiber fracture in composite materials.

However, in order to make use of the information that these emissions provide one must develop a quantitative or at least thorough qualitative understanding of the sources of acoustic emission. This understanding is complicated by a wide range of factors. These factors include the possible non-isotropic nature of the source and propagating medium, the interaction of the elastic wave with the material between the source and receiver, and finally the signal modifications inherent to the detection and analysis system. A number of approaches have been taken to overcome these difficulties and therefore, analysis of these emissions has taken many forms.

Some investigators have attempted to isolate source behavior by using a systems approach (46). That is, by formulating the appropriate transfer functions that reflect the influence on the acoustic wave by the material, receiving transducer and instrumentation. The inverse of these transfer functions is then applied to the known output signal and the source characteristics are inferred. Recently many investigators have turned to analysis of the frequency spectrum of received signals for information concerning the sources of emission. Often these investigations employ random variable statistics techniques to analyze the wave behavior (48).

Despite the continued development of these analysis techniques, AE analysis is for the most part qualitative. The recent developments in signal analysis have provided a great deal of information on the basic nature of the elastic waves which are generated inside a material however little success has been shown in quantitative evaluation of source behavior.

An example of the type of qualitative analysis which is often successfully performed on acoustic emission is shown in Table 2.1. This table, derived from similar listings frequently cited in the literature (50), shows how the amplitude of acoustic waves is affected by the emission generating process and by the material in which the waves propagate. Similarly, other AE parameters such

Table 2.1 - Source characteristics and material factors which affect AE amplitude.

Factors Which Increase AE Amplitude	Factors Which Decrease AE Amplitude
High strength	Low strength
High stiffness	Low stiffness
High strain rate	Low strain rate
Low temperature	High temperature
Brittle failure	Ductile failure
Martensitic phase transformation	Diffusion controlled phase transformation
Large grain size	Small grain size
Cast structure	Wrought structure
Crack propagation	Plastic deformation
Mechanical twinning	Thermal twinning

as duration, rise time, count rate and energy can be used to discriminate between various sources. The parameters are defined in Appendix B.

This type of qualitative analysis has been facilitated by the separation of AE activity into two basic groups: burst type activity and continuous activity. Burst type emissions result from "brittle" events such as cracking, mechanically induced twinning, and martensitic phase transformations (50). Typically, these events have high amplitude, short rise time, short duration and high energy. Continuous emission occurs following low energy type events such as dislocation motion and diffusion controlled phase transformations. Characteristically these low energy events have a long rise time, low amplitude, long duration and are very similar in nature to background noise. A schematic illustration of the difference between continuous and burst emission is shown in Figure 2.1. The use of these two general categories of emission has been used most successfully for discriminating between ductile events such as dislocation motion from brittle processes like microcracking.

Although only recent advances have made even qualitative source characterization possible, acoustic emission has been used extensively over the past 35 years. The first observations of acoustic emission in metals were made hundred years ago by tin smiths who observed the characteristic "tin cry", during deformation processes. These audible sounds were later attributed to twinning in the tin. The recent developments and interest in acoustic emission is generally attributed to the work of Kaiser in the early 1950's (50). He reported that all metals exhibited acoustic emission upon plastic deformation. Kaiser also first reported that acoustic emission was irreversible: that is, unless appreciable recovery takes place, emissions will not occur upon reloading until the previous maximum load is achieved. This phenomenon has subsequently been termed the "Kaiser effect". Kaiser however, mistakingly attributed all emissions to grain boundary sliding. It was not until later in the 50's when improved instrumentation allowed for the attribution of these emissions to dislocation activity (45). The capability for monitoring structures for ductile overload was a direct result of these investigations. Concurrent developments in acoustic emission technology resulted in widespread application of acoustic emission for the detection of fatigue crack growth, weld cracks and environmental effects on materials. In particular the use of AE for moni-

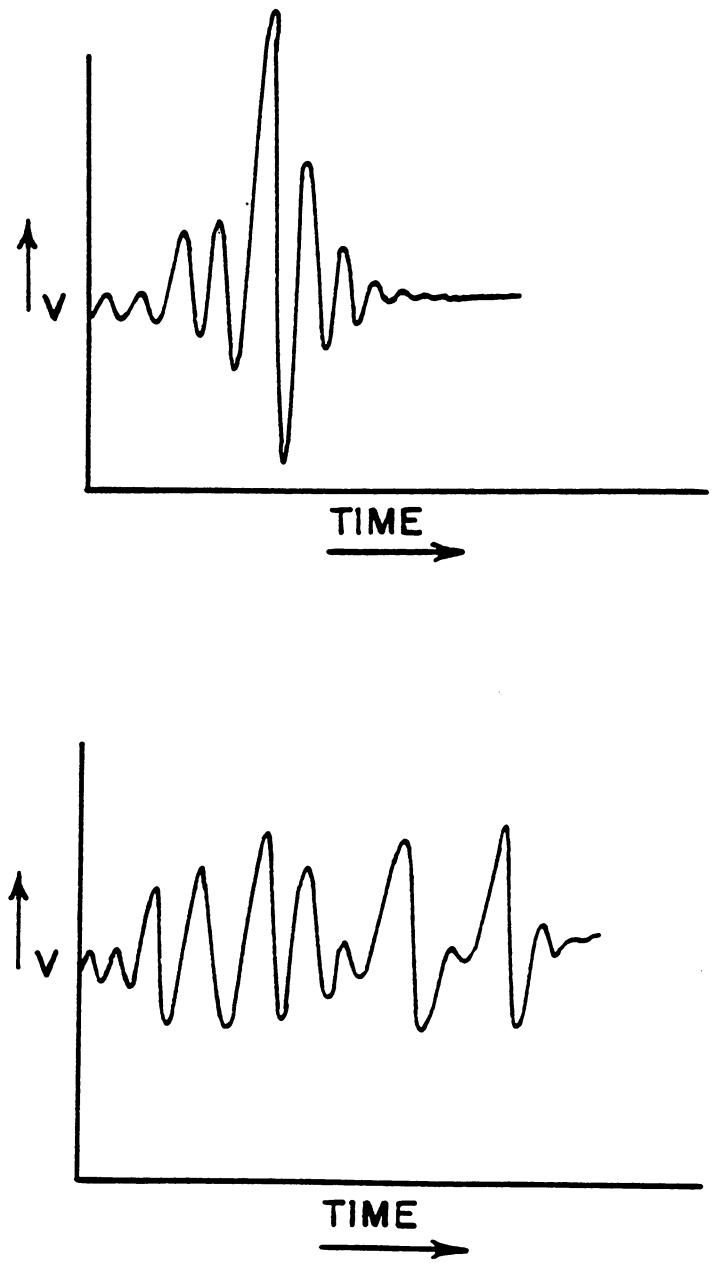

Figure 2.1. Schematic of burst (top) vs. continuous (bottom) emissions.

toring environmentally enhanced delayed failure quickly gained favor because of the significant period of detectable stable crack growth preceding failure.

In addition to monitoring the process of delayed failure in service, AE has also been used as a research tool for studying environmental effects on metals. This work has again predominantly focused on the monitoring of crack growth under controlled conditions. Specifically, Dunegan and Tetelman have used AE to determine rate of cracking in a high strength steel due to hydrogen exposure. Acoustic emission consisted of a series of small bursts followed by quiet periods. These quiet periods were thought to be related to the time required for hydrogen diffusion to the crack tip. More recently investigators have correlated the time between these small bursts of emission with diffusion times through a single grain, indicating that crack propagation occurs by grain boundary decohesion as hydrogen proceeds through the material.

Other investigators have used AE to monitor hydrogen effects on plastic flow. Acoustic emission from a high strength steel during plastic deformation was found to increase with increased hydrogen concentration (51). The presence of hydrogen was also found to eliminate the occurrence of the Kaiser effect in this alloy. These occurrences were attributed in part to locking of dislocations by hydrogen.

Understanding the manner by which dislocation motion can generate detectable acoustic emission is fundamental to using AE for the analysis of ductile processes in general and specifically in studying the effect of hydrogen on these processes.

Because of the low elastic energy released in the motion of a single dislocation, a number of dislocations within a small volume must move almost simultaneously in order to generate detectable emissions. In alloys where cross slip is difficult, precipitates serve to pin dislocations (52). At the onset of flow, many dislocations can pile up at these pinning points. If these pinning points are fairly weak, the dislocations will eventually break away. This breakaway of a large number of dislocations leads to the generation of detectable AE activity. When cross slip is not difficult, these

pile ups do not result and precipitates do not promote increased activity. The ability of dislocation to cross slip is inversely related to stacking fault energy. If the interaction of precipitates is critical to the generation of AE activity. It appears that stacking fault energy would be a material parameter that would significantly affect acoustic emission. The importance of stacking fault energy on AE in a number of FCC alloys has been investigated previously. Hatano reported that AE activity decreased with lower stacking fault energy while other investigators reported no correlation between stacking fault energy and AE activity (52). Because of the relative unimportance of stacking fault energy on the nature of flow in BCC alloys no stacking fault energy effect in these alloys is expected.

Another proposed mechanism for dislocation generated emission involves dislocation breakaway from Cottrell atmospheres. In alloys that evidence serrated yielding, the repeated breakaway of dislocations from their atmospheres has been shown to generate high levels of activity (52). In these alloys the nature of slip and hence stacking fault energy have been shown to have no effect on AE generation.

In attempting a new technique for gaining insight to the sources of emission a recent study by Clough and Wadley (53) acoustically monitored indentation loading to investigate hydrogen embrittlement in a quenched and tempered low alloy steel. Clough and Wadley observed hydrogen induced cracking beneath the indentation which they proposed to be the source of the emission. Because of the very small volume of material undergoing deformation in the indent process, this technique has proved beneficial in overcoming the previously mentioned difficulties in source characterization. In standard tensile tests, the large amount of material under stress makes assigning acoustic emission to a particular source impossible. Because the stress state around an indentation is well characterized and a small volume of material is under load, source identification is to an extent possible using the indentation technique. The monitoring of acoustic emission from an indentation had been previously used to study brittle fracture in tool steels (53,54), and glass (53,55) and stress corrosion cracking and indentation fatigue of aluminum (53,69). Although the previously mentioned tests studies were all conducted using full scale macro indentations there is no reason to assume that similar tests could not be conducted using a micro-indentation technique. Although

the magnitude of resulting emissions would decrease, the smaller volume of material undergoing deformation would offer the advantage of further aiding source identification and also make the test nondestructive. The following section discusses previous applications of microindentation techniques.

2.3 *Microindentation Techniques*

A microindentation is commonly defined as an indentation which has a diagonal of less than 100 μm (58). In general, these indentations are made with a load not exceeding 1 Kg; however, loads as small as 1g have been used (59). Microindentations have been used for microhardness testing of components which are too small or thin to be measured by conventional hardness testers, when trying to extract hardness profiles from near surface regions or when trying to isolate hardness of individual constitutents in a nonhomogeneous material. Microhardness testing also has the advantage of imparting less damage to the material being tested and thus the test is often considered to be nondestructive.

Microhardness indentations are commonly made with either a Vicker's or Knoop indenter (Figure 2.2). The Knoop and Vicker's indenter both consist of a diamond ground to a pyramidal form, the difference being that the Vicker's diamond indentation is equiaxed. Because of this geometry difference the Vicker's indentation penetrates about twice as deep into the material and is therefore less sensitive to surface effects than is the Knoop indentation (58).

Little direct investigation has been involved with the stress state around a microhardness indentation. It is widely accepted that because of geometric similarity the downward extrapolation of models developed for macroindentation to the micro level is valid. The stress field surrounding a macro indent has been discussed by many investigators, many of whom have applied Hill's ana-

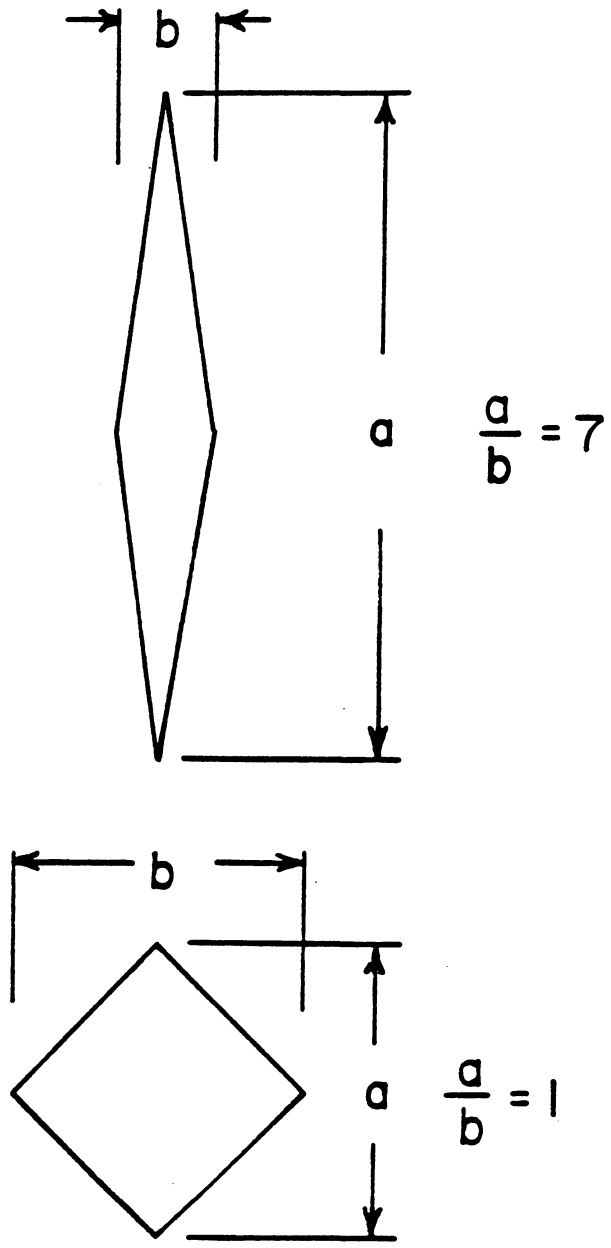

Figure 2.2. Geometry difference between Knoop (top) and Vicker's indenters.

lytical solution for an expanding spherical cavity as a model for the indentation process (53). Experimental results and more sophisticated analyses generally support this model although other investigators have discussed problems promoted by application of this model at the near surface region (60). For the purposes of this investigation the Hill model in which the volume of the indentation is accomodated by radial expansion of the material will promote its use over the more sophisticated models where radial displacement of the elastic-plastic boundary accomodates the indenter. Figure 2.3 illustrates the stress field that results under loading by the pyramidal indenter in an ideal, isotropic, elastic-plastic material. The tangential stresses that develop in the region beneath the indenter in the material are given by Hill's solution as

$$0^{P}_{\theta}\ (r) = \sigma_y\ [-2\ln(\frac{r_p}{r}) + \frac{1}{3}]\ r \leq r_p \qquad 2.4$$

where r_p is the plastic zone radius and $\sigma_y = 3^{P}_{\theta}(r_p)$, is the uniaxial yield stress. This tangential stress is known to be critical in deformation and especially in fracture processes in this region. Outside the plastic zone the elastic stress is tensile and is given by

$$\sigma^{e}_{\theta}\ (r) = \frac{1}{3}\ \sigma_y\ (\frac{r_p}{r})^3 \quad r \leq r_p \qquad 2.5$$

Thus, from the Hill model the elastic stress decreases as r^3 from the point of contact. Other investigators have suggested an r^{-2} dependence of this stress (60). A major feature evident in the Hill stress field model is the presence of stresses which span the range from compressive plastic to tensile plastic. Therefore a wide range of deformation and fracture processes are possible near an indentation. Even more complexities are evidenced when unloading occurs and the geometric size and magnitude of the tensile region beneath the indentation are increased. In fact, unloading cracks frequently result immediately beneath the indentation during microhardness indentation of brittle materials. These unloading cracks have long been considered troublesome in microhardness testing

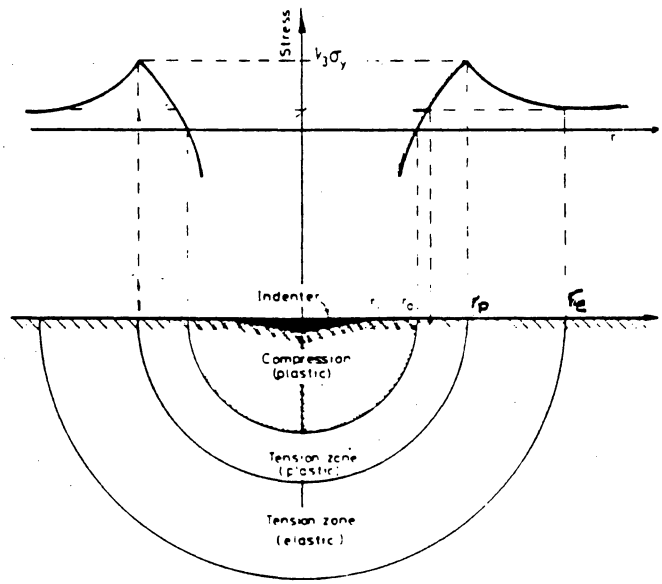

Figure 2.3. Stress field under indenter in ideal isotropic elastic/plastic material.

of brittle materials. However, within the past 10 years these cracks have led to an entire new application for microindentation. Analysis of unloading cracks has yielded quantitative information regarding fracture behavior of brittle materials (61). Measurement of lengths of radial cracks in the corners of pyramidal indenters have been correlated directly with fracture toughness. Therefore, with a single indentation in a brittle material a fracture toughness determination can be made. The well characterized crack patterns that result from indentation of these brittle materials have also been used to evaluate surface stresses (62) and for the modeling of abrasive processes (63).

Despite these applications the majority of microhardness testing has been directly involved with deformation characteristics of materials. Because microhardness is technically the resistance to penetration and continued deformation of a material, it most directly reflects the work hardening capacity of material being tested. Microhardness is therefore correlated with the ultimate strength of a material in a very straightforward manner. However, attempts to correlate yield strength with these hardness values have not been nearly as straightforward or successful. The investigation presented here attempts to further expand the application of microindentation techniques. Because microhardness testing is very sensitive to slight variations in the indent process, a microhardness tester is capable of delivering a highly reproducible, highly localized load to a material (53). This technique attempts to exploit these characteristics of the microhardness test system and use the indenter merely as a highly reproducible strain energy source for the activation of ductile and fracture processes in the material. AE activity resulting from these processes is monitored and evaluated to detect hydrogen in the material and to isolate the mechanisms by which hydrogen affects material properties.

3.0 Methods and Materials

The primary purpose of this investigation was to determine whether acoustic emission resulting from a microhardness indentation could be employed as a nondestructive test for the presence of hydrogen in metals and alloys. In order for such a test to be effective it must be shown to be sufficiently reproducible. Therefore, the system must either be immune to the effects of component geometry, surface finish, microstructure and composition, or such system factors must be understood and accounted for in the test procedure. Many of the experiments with A106 and 4340 steel were designed to isolate some of these system factors and to demonstrate the reproducibility of this non-destructive evaluation technique.

Finally, it is thought that the sources and characteristics of acoustic activity generated during microhardness indentation must be understood thoroughly in order to develop the test to its maximum potential. Indentation fracture studies of glass, in which the sources of emission are clear, were therefore conducted in order to facilitate this understanding.

All acoustic emission data in this investigation was acquired with a Physical Acoustics 3000/3104 AE data acquisition and analysis system coupled with a Leco Microhardness Indenter. Details of the data acquisition system are described in Appendix A.

3.1 Indentation studies of A106 steel

A106 steel was the primary material studied in this investigation. A106 was chosen because of the large amount of VPI data on hydrogen effects on this alloy as well as the availability of suitable test specimens, the abundance of literature on its hydrogen compatibility and because of the potential importance of its use in hydrogen transport systems (34). The composition of A106 is given in Table 3.1. Figure 3.1 shows the as-received ferritic-pearlitic microstructure typical of the test samples used.

The 1/2″ x 1/2″ x 4″ bars were heat treated to produce two structures in addition to the ferritic-pearlitic structure. A bainite-like structure, Figure 3.2, was achieved by normalizing at 900^{O}C for 2 hours, holding briefly in room temperature air and then quenching in ice water. To generate the martensitic structure shown in Figure 3.3, the bars were treated as above but were quenched without the brief hold in room air.

3.1.1 Cathodic charging

The heat treated bars were wet ground to a 60 grit finish using SiC paper, cleaned in alcohol, and stored in a dessicator until the start of testing. These uncharged bars were then tested to determine baseline hardness and AE activity levels for later comparison with hydrogen charged samples.

The bars were secured to the indenter stage with double-sided tape. This fastening technique was found to prevent the occurance of extraneous noise during microhardness testing. Each bar was indented with a 1Kg load for 10s using a Vicker's diamond pyramidal indenter. AE signals were monitored using the test system described in Appendix A. System parameters used in this test are

Table 3.1. Nominal Composition of A106 Grade B Steel.

ALLOY CONTENT, %			
C	Mn	Si	Fe
0.25 max	0.27-0.93	0.10 min.	balance

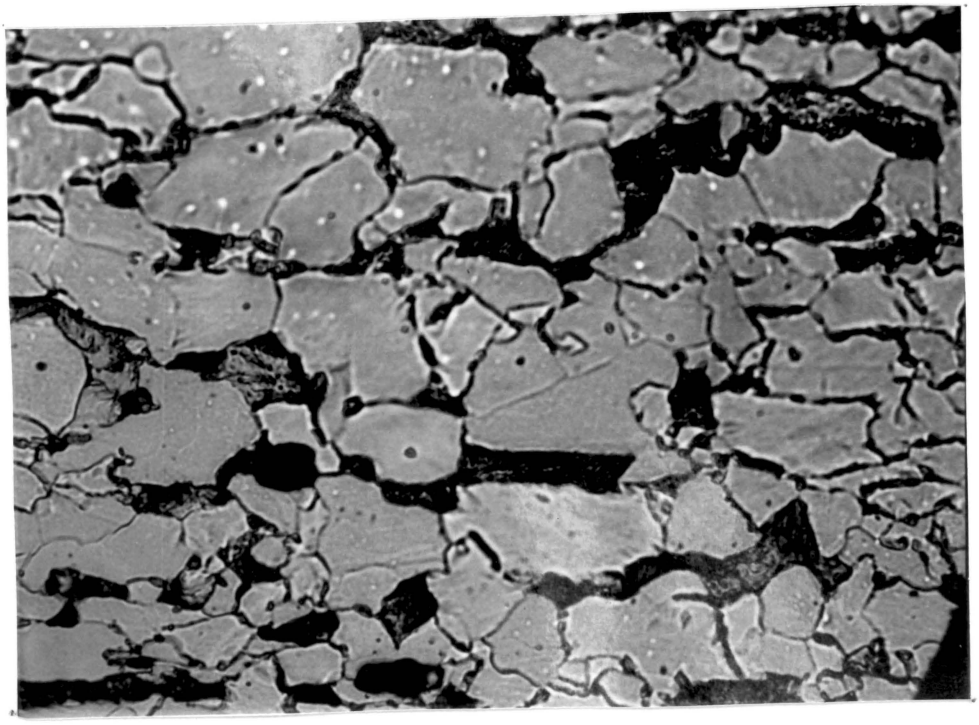

Figure 3.1. Typical ferritic/pearlitic microstructure.

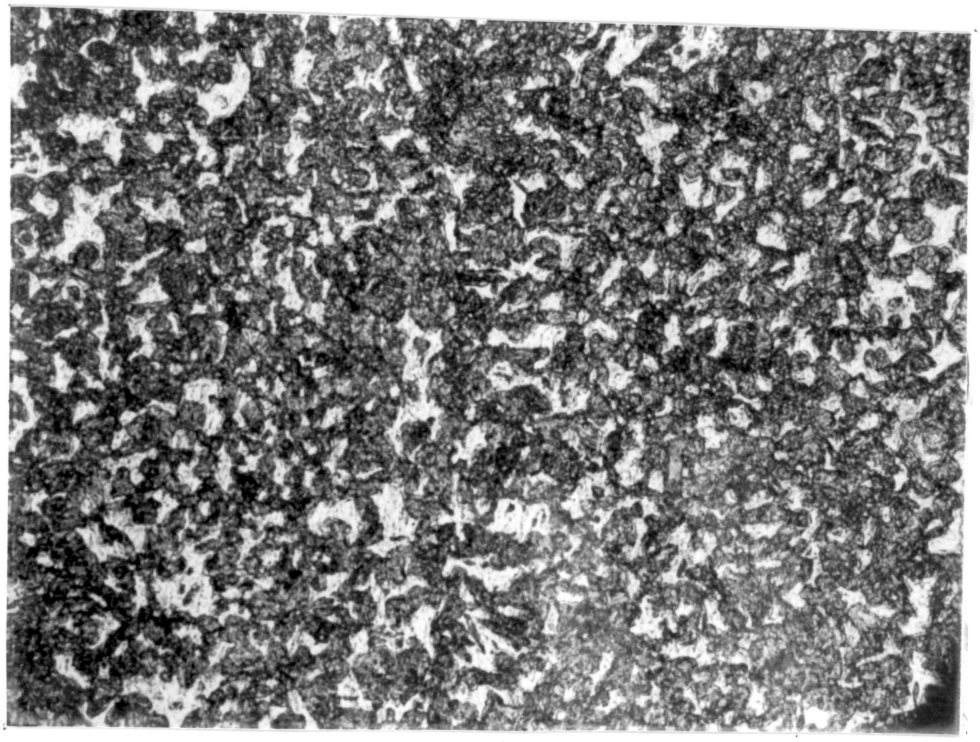

Figure 3.2. Bainite-like A106 microstructure.

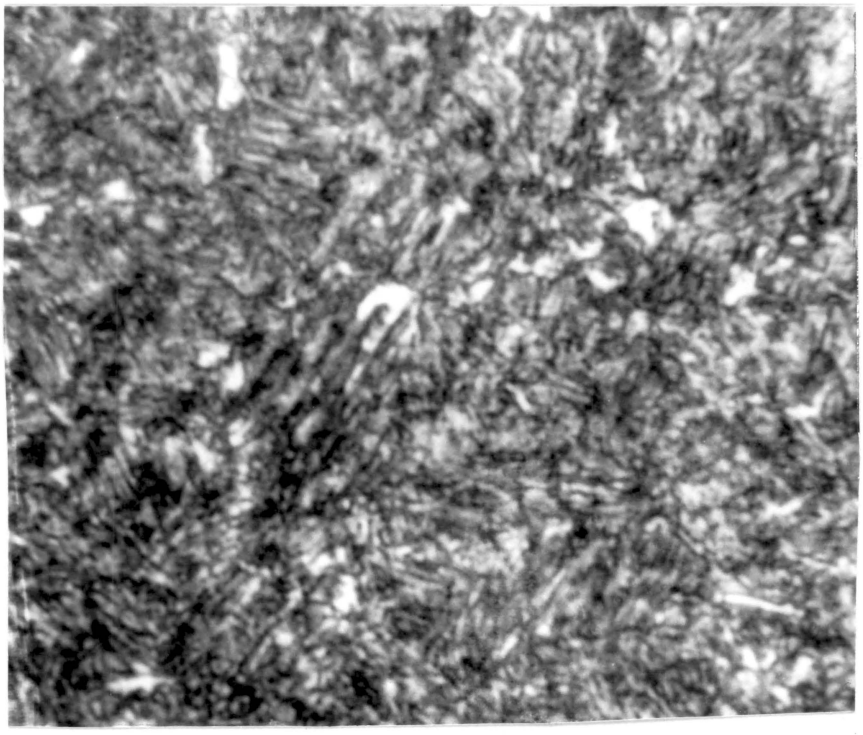

Figure 3.3. Martensitic A106 microstructure.

shown in Table 3.2 and their significance is discussed in Appendix B. The resulting data were stored on a floppy disk. Microhardness readings were also recorded.

These samples were then cathodically charged with hydrogen using the system shown in Figure 3.4. The solution consisted of 1 N NaOH with 25 g/l sodium arsenite added as a hydrogen recombination poison. Bars were charged for 2 hours at a cathodic current density of 10 mA/cm^2. After charging, the bars were rinsed in water and lightly ground with 60 grit SiC paper in order to remove any films or other surface effects which may have resulted from charging. Following an alcohol rinse, these hydrogen charged and ground bars were retested using the procedure developed for the baseline data. Testing was repeated over period of at least one week. The bars were then annealed and tested again.

3.1.2 Gaseous charging

Bars of ferritic-pearlitic A106 were chemically polished using a solution of 80 ml distilled water, 28 ml oxalic acid (100 g/l) and 4 ml hydrogen peroxide. The bars were then hydrogen charged in an autoclave at $140^{o}C$ and 400 psi for 17 days. After removal from the autoclave, the samples were stored in liquid nitrogen until testing began. The liquid nitrogen storage was used to prevent hydrogen outgassing. The indentation procedure and acoustic monitoring were then repeated after the bars were removed from storage, as before, again using the parameters shown in Table 3.2. Tests were repeated over a three week period during which the samples were stored at room temperature.

Table 3.2. System Parameters

Threshold	0.3 V
Gain	38 dB
Dead Time	1 μS
Time Base	.01 s

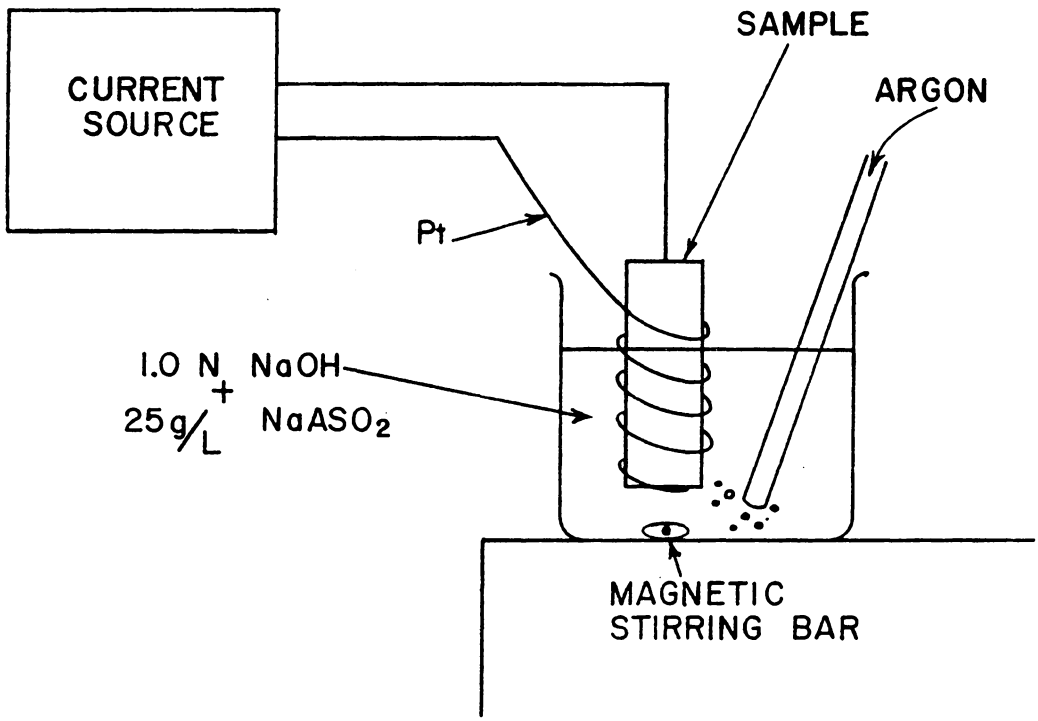

Figure 3.4. System used for cathodic charging of test samples.

3.1.3 Acid pickling

Selected ferritic pearlitic A106 bars were pickled in dilute hydrochloric acid to determine if adsorbed hydrogen resulting from a common material processing technique such as pickling would result in detectable levels of AE activity due to adsorbed hydrogen.

The bars were chemically polished by the techniques described in section 3.2 and stored at room temperature. They were then pickled in a 10% solution of HCl (36.5-38.0 assay) for 10 minutes. After removal from the solution, each sample was rinsed in water and tested immediately. Subsequent tests were then conducted almost continuously for the next twenty minutes. Test parameters were the same as those used in the cathodic and gaseous charging experiments.

Another A106 bar was ground to a 400 grit surface finish and pickled for 15 minutes in a 20% HCl solution in an attempt to increase the hydrogen absorbed by pickling. This sample was then tested in the same manner as the sample which had been pickled for 10 minutes in a 10% HCl solution.

Because of the short time involved in the pickling experiments, the pickling scale was not thoroughly removed prior to the test. Furthermore, it was not possible to conduct duplicate tests on individual samples.

3.1.4 Surface finish effects

To determine the effects of surface finish on the test results as recieved A106 bars were prepared to 60 grit, 320 grit and chemically polished surface finishes. These bars were then cathodically charged with hydrogen and tested by the procedures outlined in Section 3.2.

3.2 *Indentation of 4340 steel*

A limited number of tests were made on 4340 steel which is a high strength steel known to be highly susceptible to hydrogen embrittlement. Test bars which were 1/8″ x 3/4″ x 11/2″ were ground to 60 grit and tested by the procedures described in Section 3.2. These fully martensitic samples were evaluated to determine the potential significance of alloy type on the test results.

3.3 *Indentation of glass*

In order to study the charcteristics of acoustic emission resulting from cracking of brittle materials, microhardness indentation with AE monitoring was performed on glass plates.

Glass plates which were 3″ x 3″ x 1/4″ were cleaned, secured to the indenter stage and indented with a 1Kg load for 10s. The indentation process was monitored as previously with the system parameters given in Table 3.2. A number of trials were conducted and the resulting cracks were observed and photographed.

4.0 Results and Discussion

During analysis of acoustic emission resulting from the microhardness indentations most of the event parameters discussed in Appendix B were considered. However, the discussion in this text will focus primarily on the use of the energy parameter. This parameter was chosen because it has been found to be less sensitive to geometry, differences in propagating media, and system parameters than are, for example, counts and amplitude. Energy, and in particular log energy (64), has also been found to be more closely identified with the processes which generate emission, whether these processes are related to the release of surface energy during cracking or to the activation of dislocation sources. This association between anticipated processes and energy make energy more suitable for quantitative analysis of AE activity than other parameters such as amplitude, rise time, and duration. These latter parameters are used primarily for qualitative source characterization.

4.1 Indentation of Ferritic-Pearlitic A106 steel

4.1.1 Typical results

The typical acoustic emission during a microhardness test of the A106 bars which had been either cathodically or gaseously charged with hydrogen are shown in Tables 4.1 and 4.2. Typically, the tests before charging showed a relatively low level of AE energy per indent. This level, calculated by summing energy from all of the events which follow an indentation, increased by an order of magnitude after charging. The AE energy per indent then decreased over time to an almost constant level which was somewhat higher than the level found in the precharge samples. An anneal then restored the sample to its precharge level of indentation activity. Due to the large amount of scatter in the data, numerous trials were performed. The data shown are average values for up to ten tests at a given time. The difference between precharge and post anneal energy levels is not significant relative to the degree of scatter. The fact that the energy did not drop to precharge levels until after annealing indicates that hydrogen is being trapped at reversible trapping sites such as dislocations and grain boundaries. These traps are clearly reversible because the annealing procedure would not have been sufficient to remove hydrogen from deep (or irreversible) trapping sites.

Hardness remained constant at approximately 180 Vdph throughout all of the tests except for a slight increase to 200 Vdph immediatly following gaseous charging.

4.1.2 Calculation of diffusivity

The graphs shown in Figures 4.1 and 4.2 illustrate an apparent exponential decay in AE energy with time. This is confirmed in Fiqure 4.3 which shows a linear relationship on a logarithmic scale

Table 4.1. Typical Data Following Cathodic Charging of A106. Data Represent Average Energy per Indent for 10 Indents at each time.

Condition of Bar	Average AE Energy Per Indentation
Uncharged	15
Immediately after charge	119
One day after charge	47
Two days	46
Eight days	41
After anneal	9

Table 4.2. Typical Data Following Gaseous Charge of A106. Data Represent Average Energy per Indent for 10 indentations at each time.

Time After Removal from Storage Bath (days)	Average AE Energy Per Indentation
Immediately following removal	49
1	127
3	82
5	78
13	57
20	26

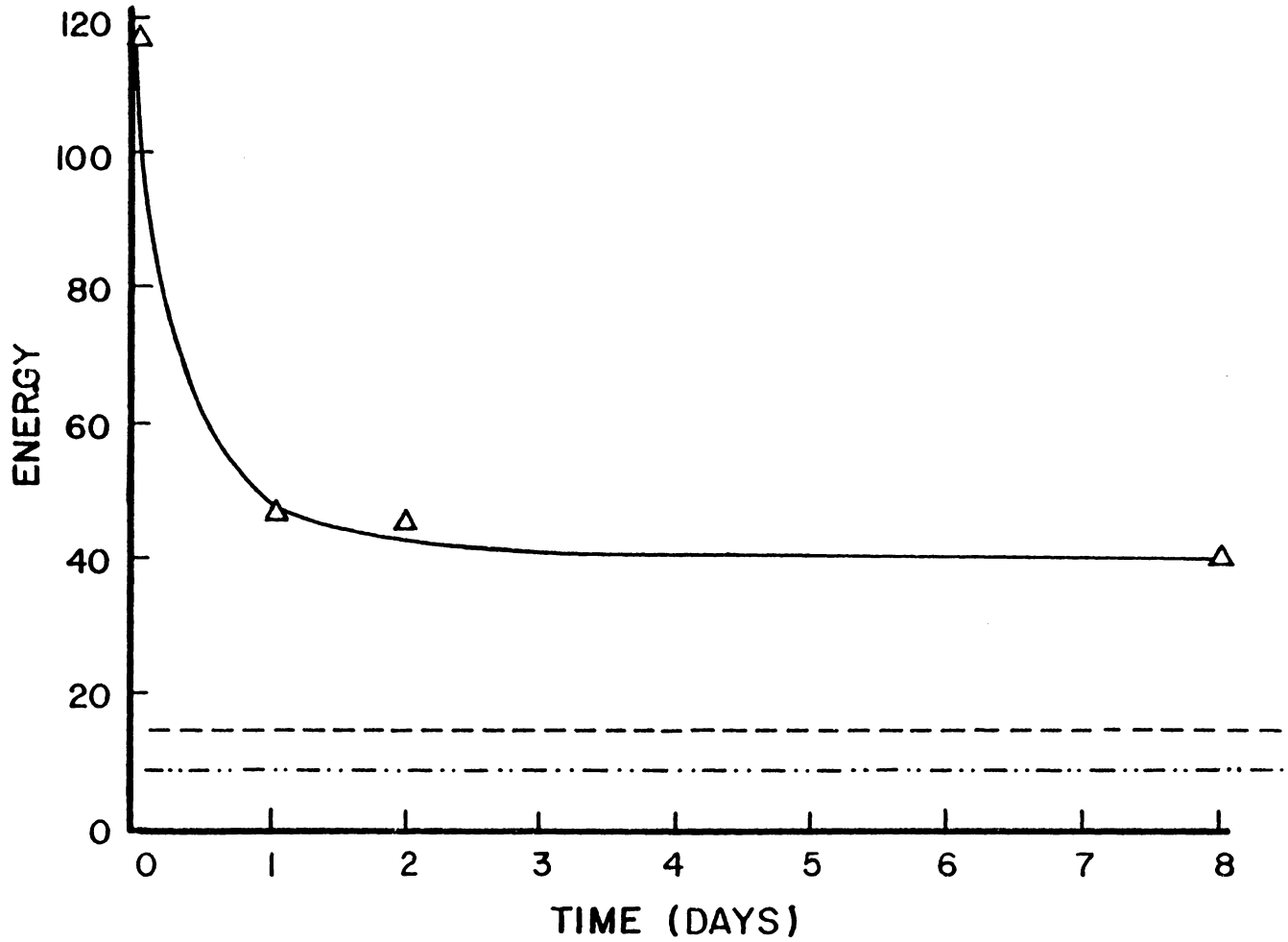

Figure 4.1. AE energy as a function of time after cathodic charging.

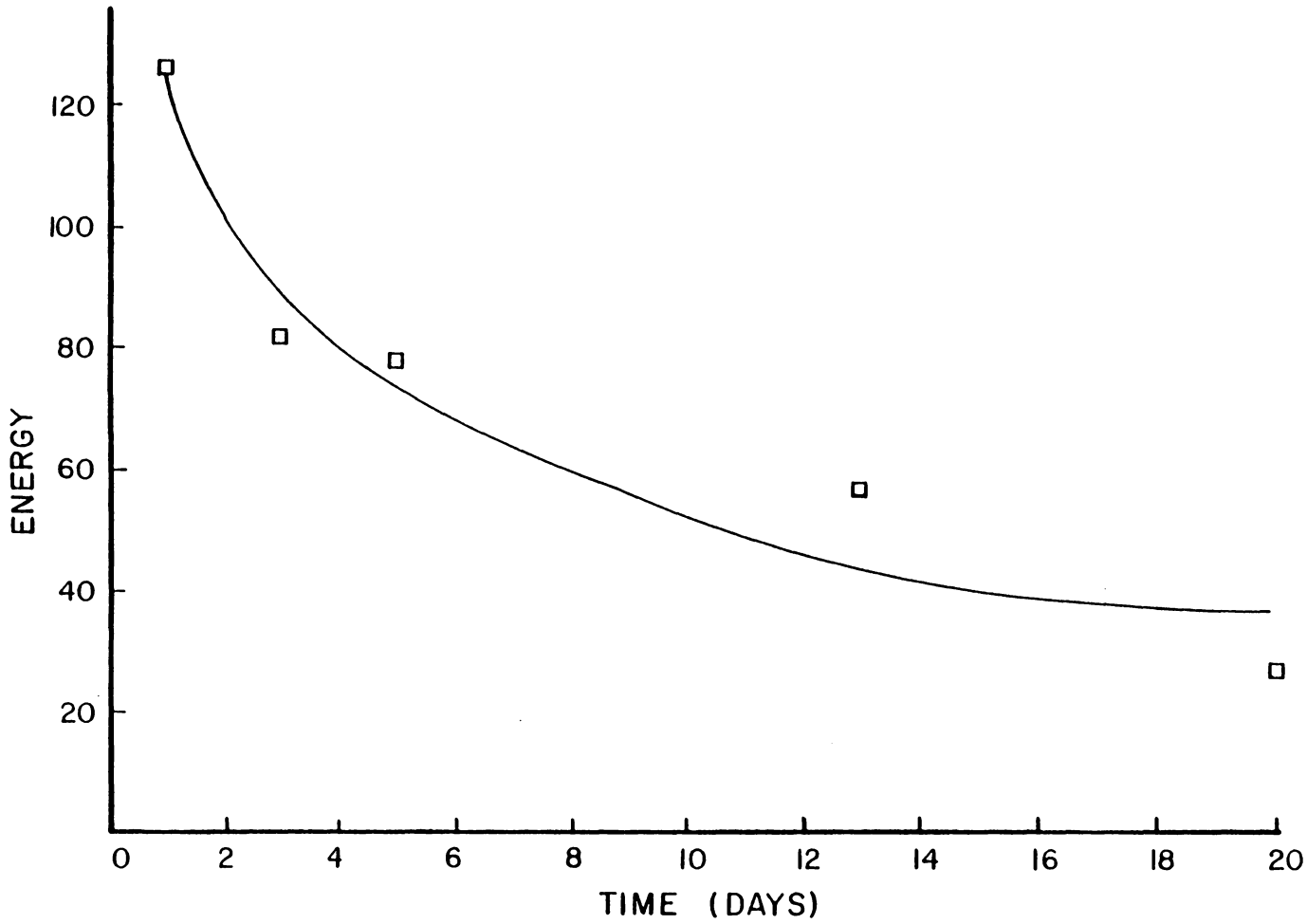

Figure 4.2. AE energy as a function time for gaseous charging.

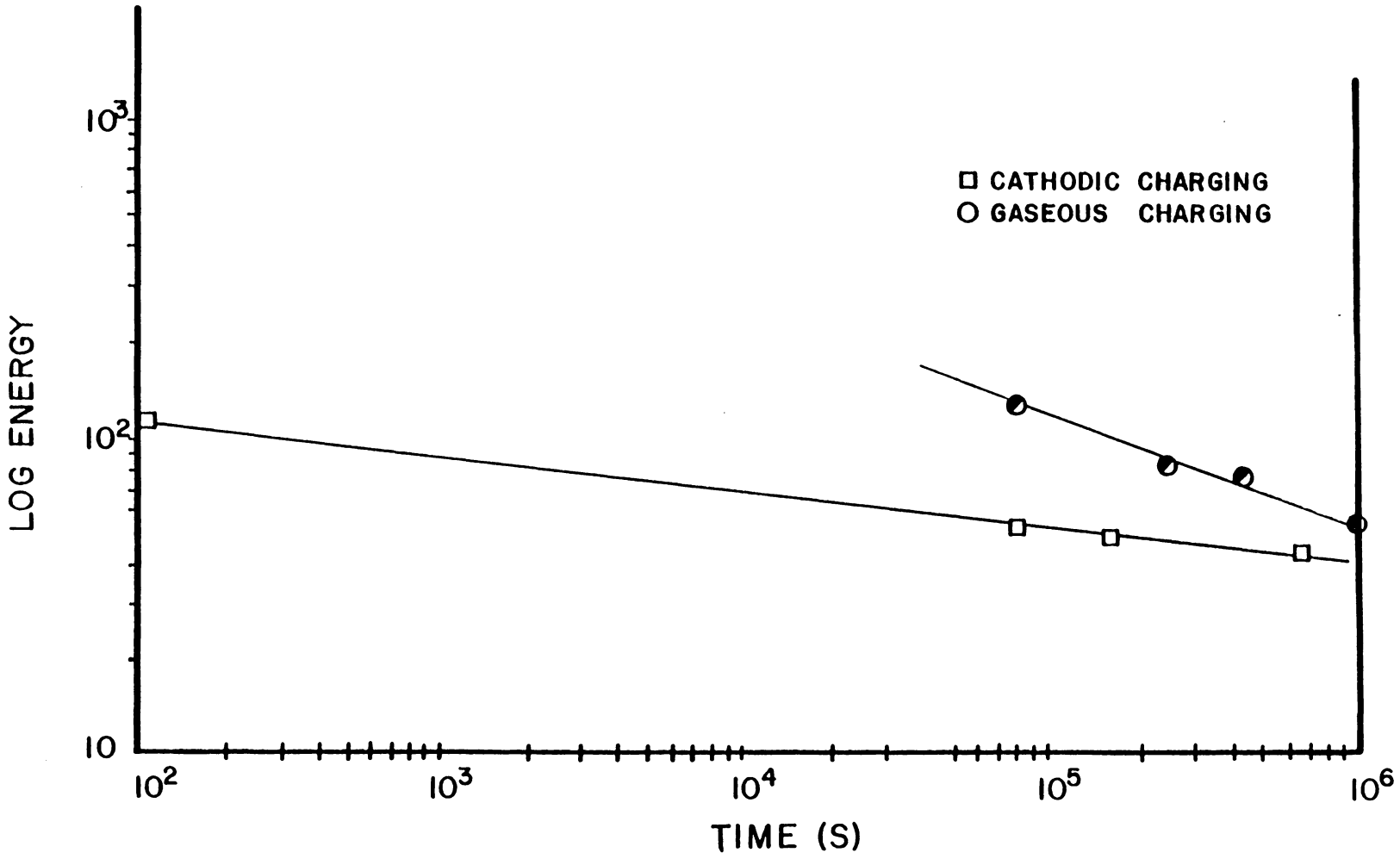

Figure 4.3. Logarithmic plot of AE energy as a function of time

for both cathodically and gaseously charged samples. The deviation from linearity of the first point in Figure 4.3 should be noted and will be discussed later. The logarithmic behavior indicates that the emission generating process may be heavily dependent on hydrogen concentration and that the continued decrease in AE energy may be controlled by the diffusion of hydrogen from the charged sample. If this is the case, in theory, a diffusivity can be calculated based on the graph of AE energy versus time. The basis for this analysis is the relatively well defined technique which dealt directly with concentrations of the diffusing species under conditions where the variations in concentrations were determined experimentally (65).

Because of relatively short diffusion times and low hydrogen fugacities used in these experiments, the use of the diffusion equation for a semi-infinite plate is justified for these bars (66). The standard semi infinite plate diffusion equation is:

$$C = C_o \ \mathrm{erfc} \left(\frac{x}{\sqrt{4Dt}} \right) \qquad 4.1$$

where C = the concentration at point x and time, t, C_o is the surface concentration and D the diffusivity. If one assumes that AE energy is directly proportional to hydrogen concentration, the slope of energy plotted against the inverse square root of time on probability paper will allow for the calculation of an approximate diffusivity. For cathodic charging this plot is showith depth into n in Figure 4.4. The detectability of any AE source will decay exponentially with depth into the sample (67), as will the intensity of the indentation stress field which will activate AE sources. Therefore, there exists a rapidly decreasing distribution of detected sources through the plastic zone. Because of this non-uniform source distribution, the average depth of AE emission was assumed to be at 1/10 the depth of the plastic zone surrounding the indentation, a reasonable if not rigorous assumption. From the Hill indentation stress field model this depth was calculated to be 3x10 m. Using this depth as X in Equation 4.1, the slope of the probability plot then yields a calculated diffusivity of 6x10 cm /s. This value is well within the range of previously determined trapped diffusivities for hydrogen in mild steels.

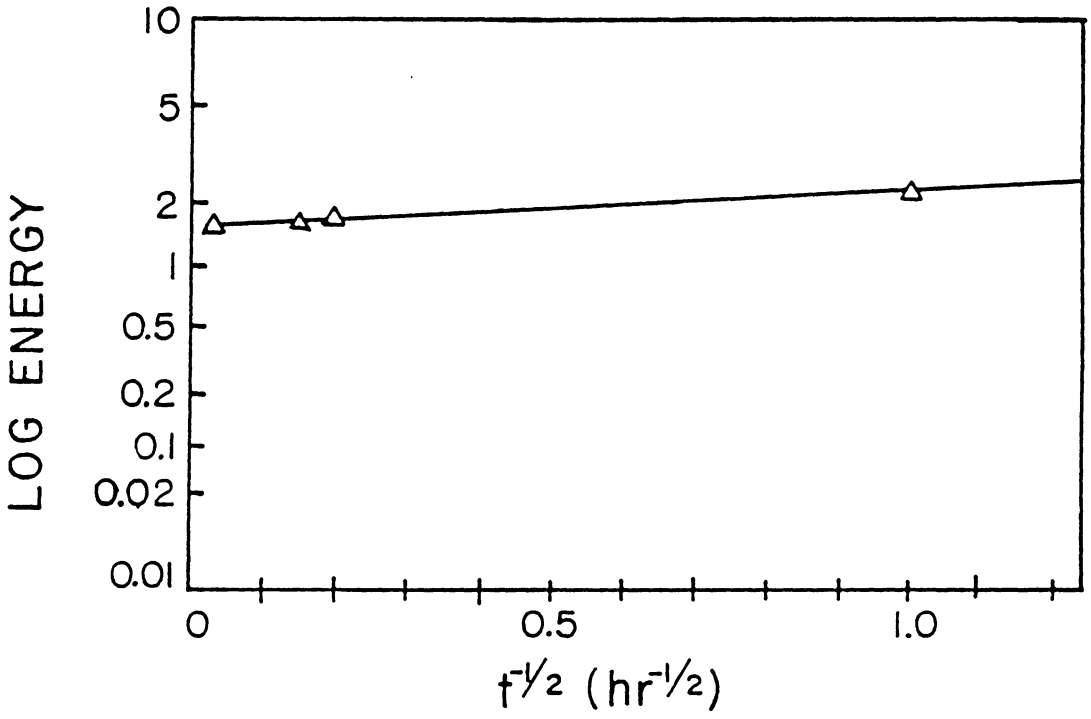

Figure 4.4. Probability plot of log AE energy as a function of time for cathodic charging.

Taking this procedure one step farther, one can assume that the primary trapping sites are dislocations. Then the relationship:

$$D_A = D_T \exp\left(\frac{G_B}{RT}\right) \qquad 4.2$$

where D_A is the actual diffusivity, D_T is the theoretical untrapped diffusivity, G_B represents the binding energy, R is Boltzman's constant and T the temperature can be used to calculate a binding energy for hydrogen to dislocations. D_T can be calculated from the relation (19)

$$D_T = 0.8 \times 10^{-3} \exp\left(1900/RT\right) \qquad 4.3$$

and is equal to $3.2 \times 10^{-5} cm^2/s$ for these room temperature tests. Substituting into equation 4.2 yields a binding energy of 2350 cal/mole. This value is in excellent agreement with binding energies calculated in previous investigations with A106 steel (69).

Analysis of the gaseous charging case would be expected to generate similar values for D_a and G_B The slope of the probability plot for this case, Figure 4.5, results in a diffusivity of $2.4 \times 10^{-6} cm^2/sec$ which is, relative to ranges of values commonly dealt with in diffusion data, identical to that which was previously calculated.

From the above calculations it appears that this technique may be useful in the calculation of various diffusion parameters; however, for the purposes of this investigation the details of the above calculations are of secondary importance to the fact that the AE generating process is clearly diffusion controlled and related in some manner to the hydrogen concentration in the sample.

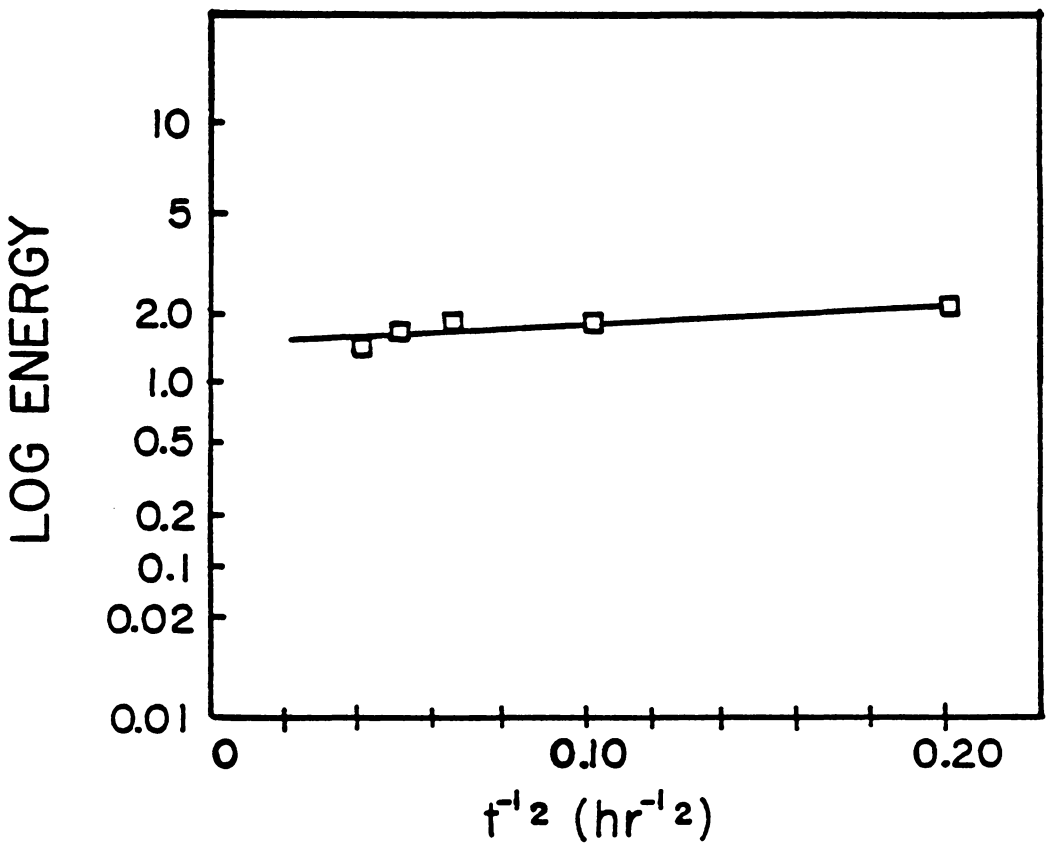

Figure 4.5. Probability plot of log AE energy as a function of time for gaseous charging.

4.1.3 Sources of activity

When considering the mechanism of AE generation in this alloy two processes come to mind. The activity could result from dislocation motion or from microcracking in the vicinity of the indentation. Previous investigators have acoustically monitored the indentation process of hard (> Rc 50) steels and proposed that the signals were generated by the formation of subsurface penny-shaped median cracks (53). These cracks were visible, after sectioning, via optical and scanning electron microscopy (SEM). These previous studies involved loads of up to 100 Kg. The much lower loads and softer materials used in this study made the possibility of cracking appear unlikely. Indeed, no evidence of cracks was found following sectioning and microscopy of several indents. Figures 4.6 and 4.7 show SEM and optical micrographs of one of these sections. The absence of visible cracking in the A106 and the lack of significant emission from the harder, less ductile 4340 and martensitic A106 (discussed later in section 4.4) appear to confirm that the source of AE is not hydrogen induced interfacial separation. Rather, it does indicate that some form of dislocation interaction with hydrogen is likely to be responsible for the activity.

The final evidence of dislocation generated emission is gained through the qualitative analysis of AE parameters. Cracking can be considered to have burst type emissions. These burst emissions tend to have large amplitude, short duration, and short rise time. Section 2.2 and Appendix B also discuss the effect that source magnitude and propagating medium have on these AE parameters. Ideally, some combination of these parameters would allow for discrimination between brittle events and dislocation sources. Previous analysis of mechanical twinning in zinc, plastic deformation in aluminum, and fracture of glass has indicated that the parameters amplitude and rise time may best serve to discriminate between the two types of activity. Indentation of glass plates resulted in cracking upon unloading, as shown in Figure 4.8. A plot of AE activity resulting from this cracking is shown in Figures 4.9. In this figure, the uncircled data points represent emissions from extraneous sources during loading. These sources may be indenter friction on the surface or sliding of the glass plate and are likely to possess the characteristics of continuous emission. This figure

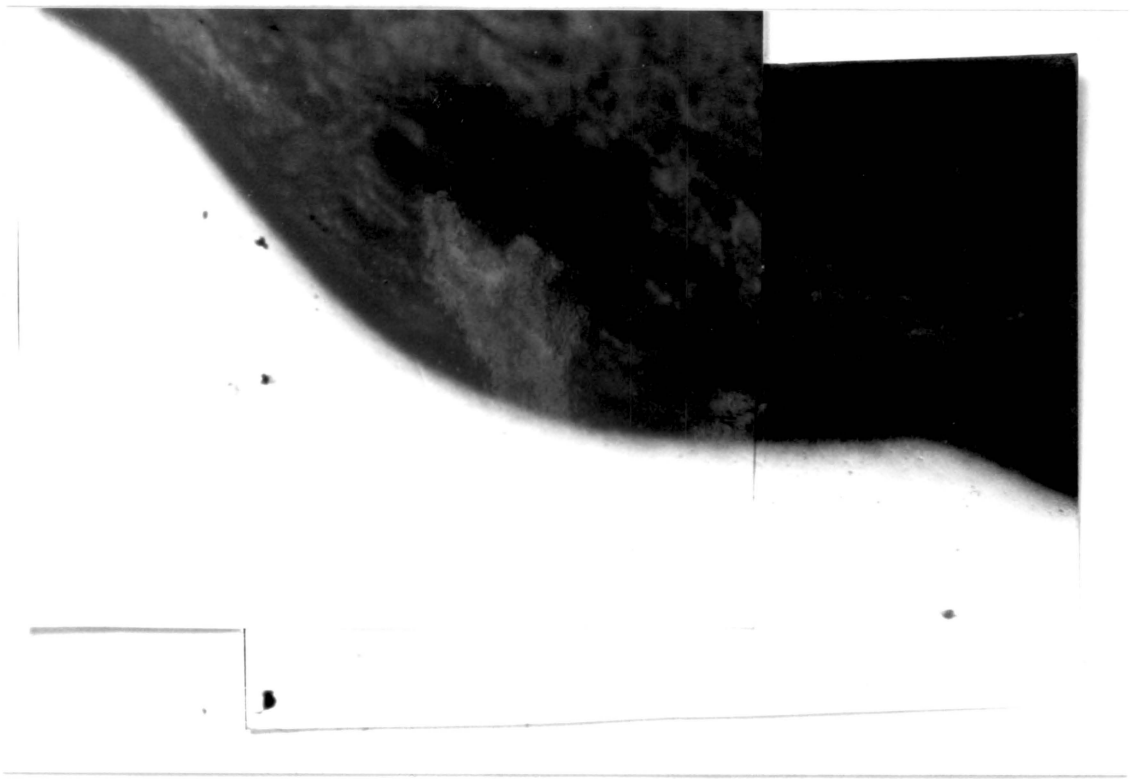

Figure 4.6. Optical photomicrograph of indent cross-section A106 Grade B Steel (250X).

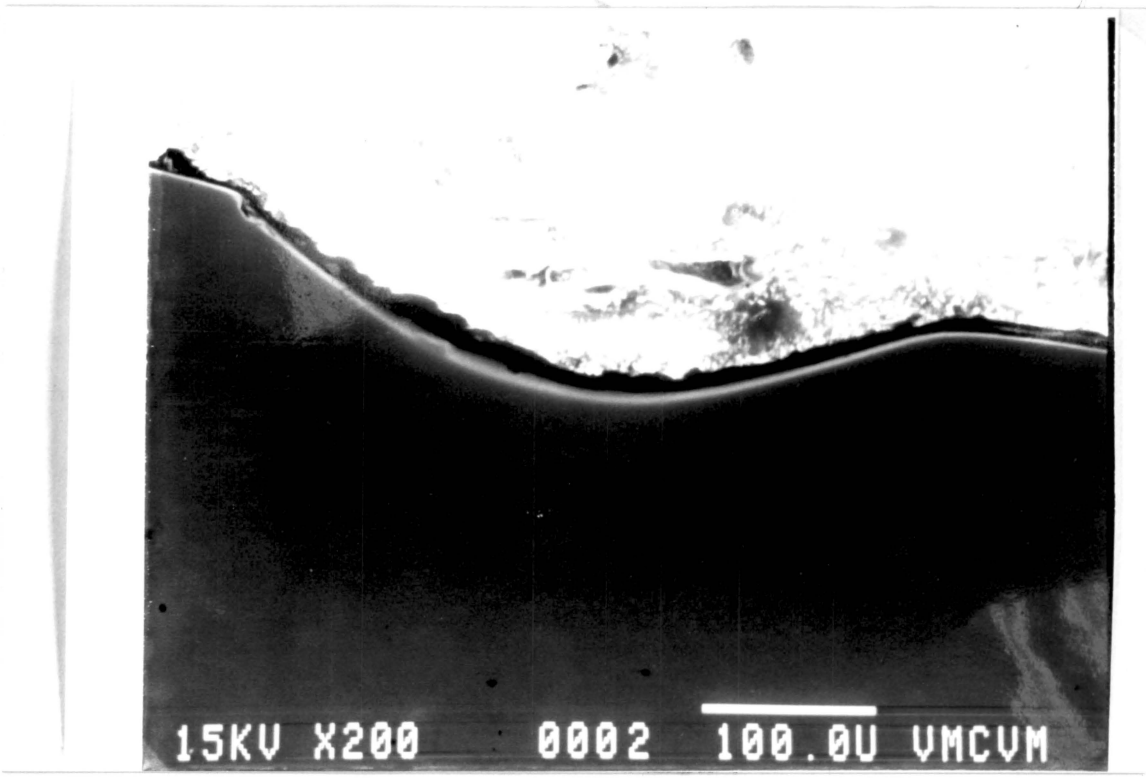

Figure 4.7. SEM photomicrograph of indent cross-section in A106 Grade B steel (200X).

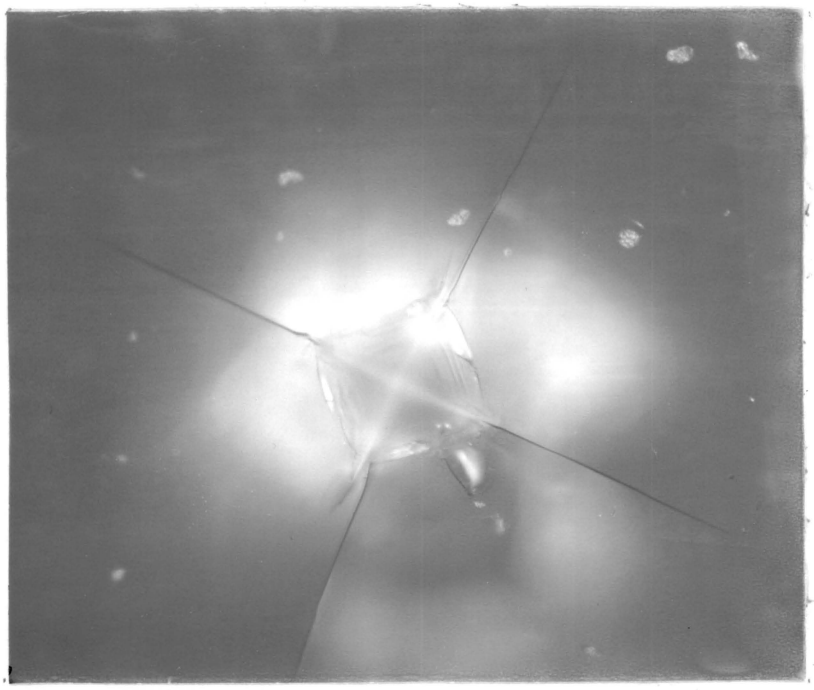

Figure 4.8. Optical photomicrograph of unloading cracks following indentation of glass plates.

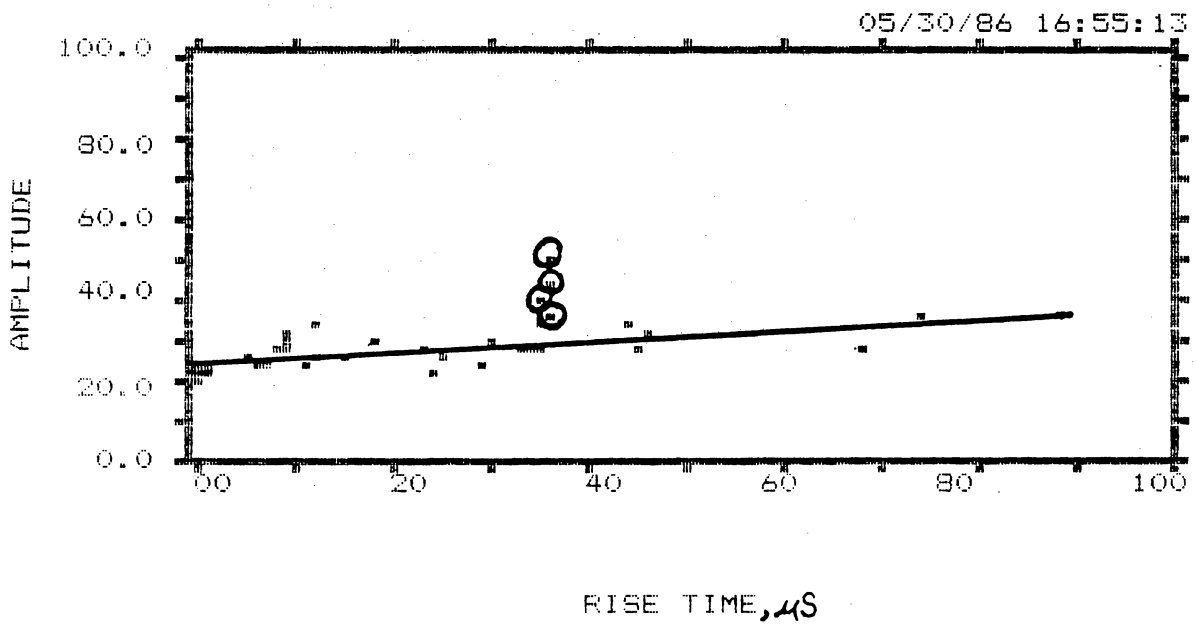

Figure 4.9. AE amplitude plotted against rise time from data following indentation of glass plates. Circled points represent unloading crack emissions.

indicates that for continuous emission sources the amplitude and rise time are clearly related. The higher amplitude events possess higher rise times and this relation is approximately linear. However, the burst type emission which results from the unloading cracks in the glass, indicated in Figure 4.9 by circled points, lie well above this line.

This analysis can be applied to the emission from charged and uncharged A106 bars. Figures 4.10 and 4.11 show that, although differing in number, the events in the charged case appear similar to that of the uncharged case. This similarity is evidenced by the slopes of the two plots, which are practically identical. In both cases there are few, if any, points which do not lie on this line. Qualitative analysis of these AE parameters indicates that cracking is not the major source of activity and that the sources of emission in the charged and uncharged conditions are very much related. Therefore, based on the continuous nature of the emission, lack of visible cracking, and all of the previous diffusion related analysis it seems very clear that the predominant source of AE activity in these tests is associated with dislocation motion.

4.1.4 Mechanism of AE generation

The previous discussion indicates that following charging, hydrogen is in some manner interacting with dislocations. This interaction leads to the release of significant elastic energy when the indenter load is applied. A proposed mechanism for the generation of this activity is that hydrogen is undergoing directed diffusion via Cottrell type locking to dislocations. Hydrogen is not being carried directly by the dislocation for such movement would be silent. Rather, the dislocation breaks away from its hydrogen atmosphere, moves a short distance, and the hydrogen then "catches up" to the dislocation via Fickian type diffusion. This model proposes that in a material, hydrogen acts in a manner very similar to carbon atmospheres which pin dislocations in Fe-C systems. This pinning by carbon is evidenced by the Portevin-LeChatelier effect or serrated yielding seen in many Fe-C alloys, Figure 4.12. Serrated yielding is a direct result of load drops which occur when dis-

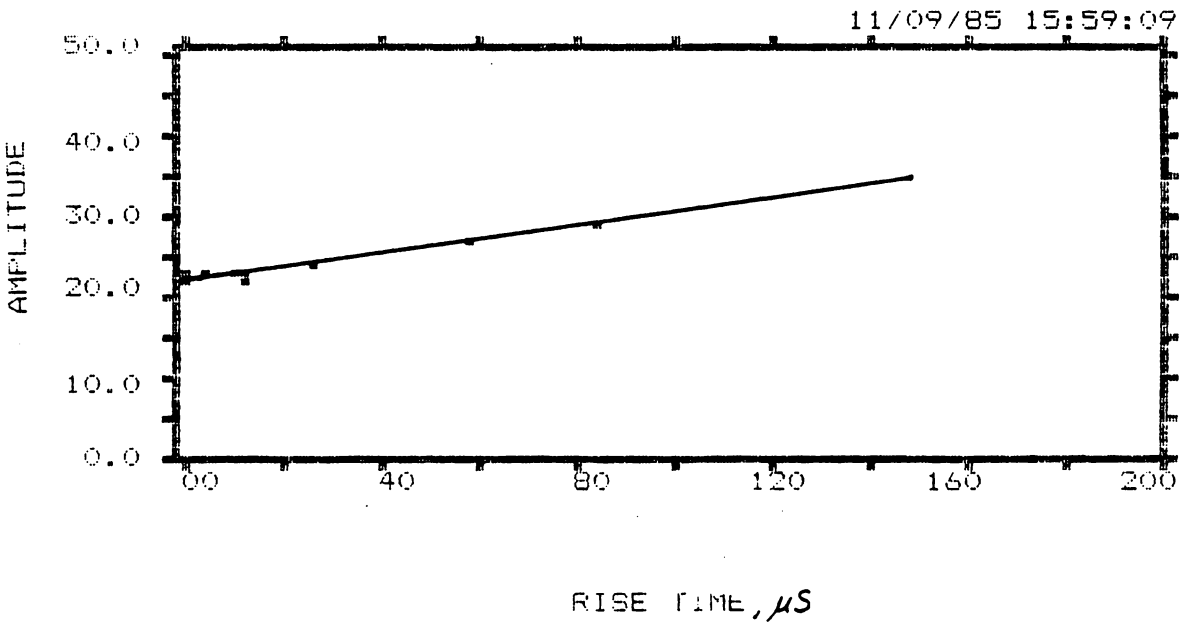

Figure 4.10. AE amplitude plotted against rise time from data following indentation of precharge A106 sample Slope is from Figure 4.9.

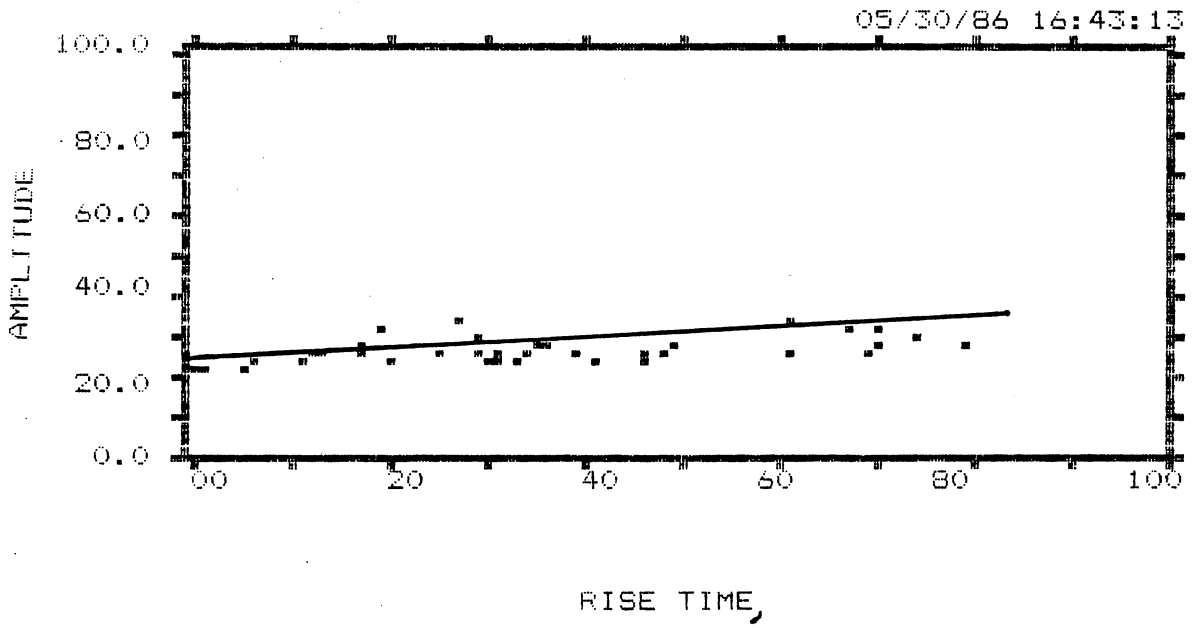

Figure 4.11. AE amplitude plotted against rise time from data following indentation of A106 sample after charging. Slope is from Figure 4.9.

locations break away from carbon pinning points. The freed dislocations are soon slowed by encountering obstacles such as grain boundaries and other dislocations. Carbon atmospheres can then be replenished and the load rises as the replenished atmospheres again prohibit dislocation movement (70). High levels of emission occur in alloys which exhibit the Portevin-LeChatlier effect. The dislocation breakaway releases an amount of energy equal to the binding energy of the atmosphere to the dislocation. A portion of this energy would be in the form of elastic acoustic waves, Figure 4.13. A similar mechanism for AE generation by dislocation breakaway from pinning points in LiF has been proposed previously (72).

The breakaway of one dislocation from a hydrogen atmosphere or any other pinning point would not be likely to generate sufficient elastic energy to be detected by any available AE detection system. Therefore, some form of internal amplification must be postulated to account for the detectability of these waves. The motion of each dislocation line segment must occur in a manner compatible with neighboring dislocation stress fields. Thus, due to the periodic nature of the crystal lattice, the vibrational waves produced by each of the dislocation line segments will tend to be in phase will interfere constructively (71). This constructive interference will in essence amplify the resulting elastic waves. Other investigators have proposed that the breakaway of a single dislocation can trigger the release of other dislocations, amplifying the signal, in a sort of "avalanche effect" (72).

At moderate concentrations, the hydrogen atmospheres do not significantly reduce dislocation mobility. This is evidenced by the lack of change in hardness data after charging. However, because hardness is more closely related to strain hardening than flow stress, the effect of hydrogen atmospheres on the onset of flow would not necessarily be reflected in hardness data. At moderate concentrations, hydrogen is unable to lock dislocations once flow has commenced; strain hardening and thus hardness are not affected.

At higher concentrations more substantial effects on dislocation mobility may be noted. In the gaseous charging experiment, testing immediately after removal from the liquid nitrogen storage bath yielded markedly less activity and slightly higher hardness than were recorded at later times.

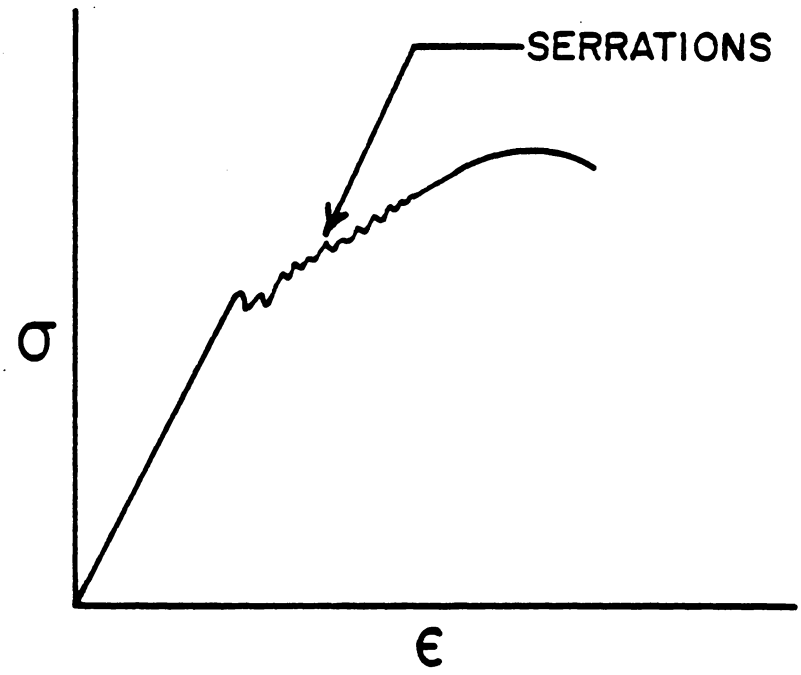

Figure 4.12. Schematic of serrated yielding seen in some Fe-C alloys.

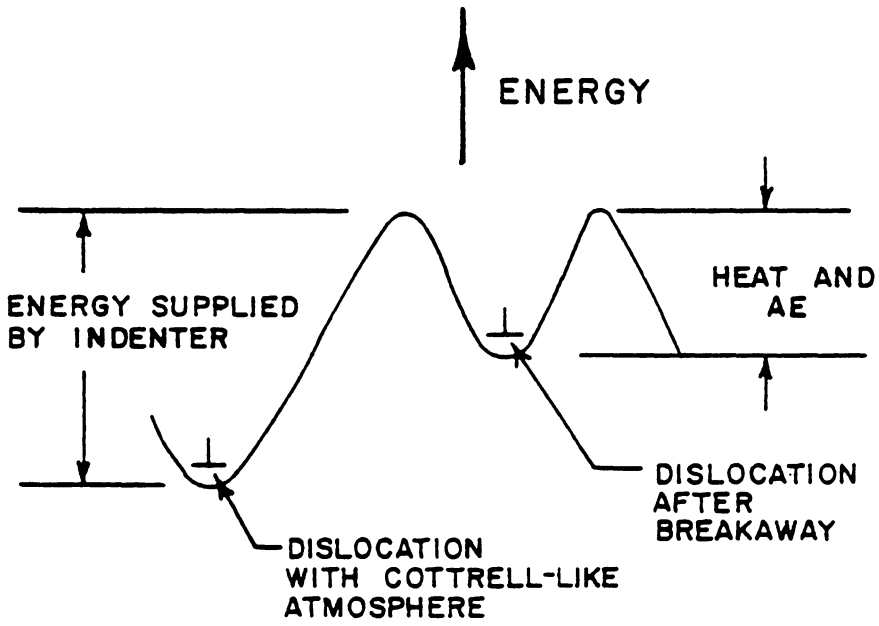

Figure 4.13. Schematic of energy of dislocation/hydrogen atmosphere system.

It is possible that the decrease in activity was caused by the higher hydrogen concentrations and subsequent decreased mobility of dislocations.

These data therefore suggest that hydrogen interaction with dislocations is having some influence on the energy involved with the onset of plastic flow. Hydrogen has previously been found to impede the onset of flow and therefore, raise the yield stress of A106 and some other alloys. Results shown here seem to substantiate these previous studies and lead credence to those hydrogen embrittlement theories based on a hydrogen induced increase in flow stress. Because the presence of hydrogen may be an impediment to the onset of plastic flow and because hydrogen has also been found to reduce interfacial strengths, these results suggest that hydrogen induced brittle fracture is more likely than hydrogen enhancement of ductile failure processes. The manner by which flow and fracture compete for dominance of the fracture process is illustrated schematically in Fig. 4.14.

4.2 Indentation of 4340 and altered A106 microstructures

4.2.1 Typical results

The tests conducted on the 4340 steel samples generated little or no acoustic activity before and after charging. The activity levels were on the order of background noise and therefore, no analysis could be conducted. This was also the case for bainite-like and martensitic A106 microstructures. As would be expected all of these microstructures were significantly harder than the ferritic-pearlitic, as-received A106 (Table 4.3). Possible justifications for this lack of AE activity are discussed in the following sections.

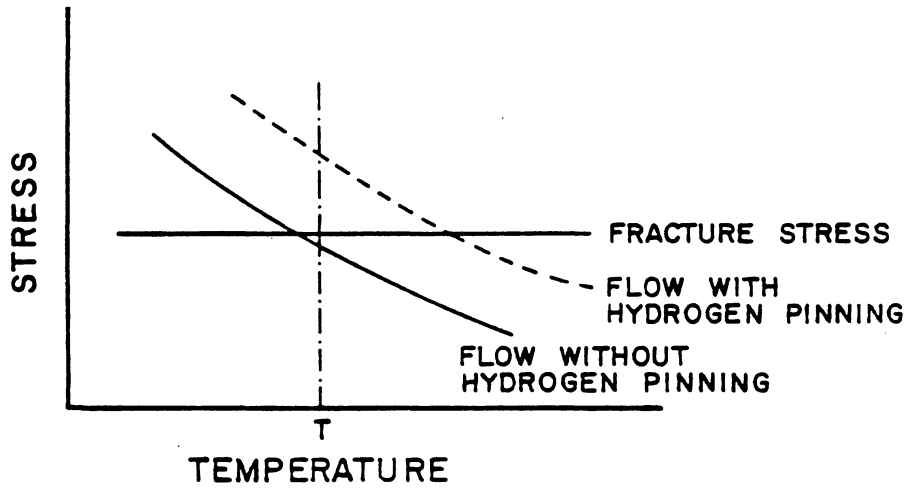

Figure 4.14. Schematic illustrating competing processes of flow and fracture.

Table 4.3. Effect of Hydrogen Charging on Hardness of Materials Tested.

Material and Condition	Hardness: Vicker's DPH Before Charge	Hardness: 1 Kg, 10s After Charge
Ferritic/Pearlitic A106	180	180
Bainite-like A106	224	224
Martensitic A106	239	300
4340	410	N/A

4.2.2 Microstructural effects on AE sources

One possible reason for this lack of activity lies in the dispersed structure of these materials. The strain fields of dislocations, in addition to interacting with hydrogen atmospheres, are influenced by the presence of dispersed carbides. These carbides act to substantially limit dislocation mobility, as indicated by the higher hardness of these materials. Because dislocation mobility is reduced, breakaway of dislocations from hydrogen atmospheres and other pinning points may not occur. It has been shown that a large number of dislocation sources must be activated in order to generate detectable activity. The dispersed structure limits dislocation mobility to such a degree that the number of activated sources is not sufficient to exceed background noise levels.

4.2.3 Indentation mechanics in hard structures

Another possible reason for the lack of detectable emissions is based on the mechanics of the indentation process. Section 2.3 briefly discusses the Hill indentation stress field model, proposed by Evans. Based on this analysis, the maximum depth of plastic deformation and thus the maximum possible depth of AE source activation is given by:

$$r_p = r_i \left[\frac{E}{3(1-\nu)\sigma_7}\right]^{1/3}$$

Substituting values in the above equation results in the values shown in Table 4.4 for the various structures. The value, r_p, is important because it is only the concentration within the volume contained by r_p which will affect the generation of AE activity. Table 4.4 indicates that this depth is significantly less in the harder materials.

Free energy considerations indicate that the hydrogen concentration of the near surface of the material is depleted. Because of the low hydrogen concentration outside of the sample, hydrogen dif-

Table 4.4. Indentation Radius and Approximate Plastic Zone Radius in Materials Tested.

	r_i	r_p
Ferritic-Pearlitic A106	0.0508 mm	.356 mm
Bainite-like A106	0.0455 mm	.273 mm
Martensitic A106	0.0393 mm	.236 mm
4340	0.0328 mm	.189 mm

fusion from the near surface region to the outside atmosphere (outgassing) will occur very rapidly. The depletion of the near surface results because replenishment of this region from inside the material does not occur as rapidly as does outgassing. A schematic of the concentration profile resulting from this near surface outgassing is shown in Figure 4.15. If, due to the higher hardness, the depth r_p is less than r_m, the lack of a necessary critical hydrogen concentration would result in these low activity levels. Figure 4.16 illustrates a computed approximation for the profile which develops during outgassing (73). Although the complexity of the mathematical analysis of such near surface effects did not allow for its inclusion in this discussion, these effects clearly need to be considered in later development of this technique.

4.3 Practical implications

The primary goal of this investigation was the developing of this indentation technique to assess hydrogen embrittlement potential in a steel. The results of this study show that at a load of 1 Kg this indentation technique may not be suitable for use with hard materials. If either, or both, of the proposed reasons for this lack of activity are valid, the use of higher loads would remedy the problem. The higher loads would extend the indentation deeper into the material and also supply more energy to initiate dislocation breakaway. Because 1 Kg is the maximum load on the available microhardness tester this could not be verified. The use of a 150 Kg load on a Rockwell indenter did yield high activity levels even in uncharged samples. However, previous investigators have shown that the use of higher loads may result in microcracking beneath the indentation (53). The degree of cracking would likely be enhanced by the presence of hydrogen. The cracking would also be expected to generate very high activity levels. Therefore, the indentation test would still indicate the presence of hydrogen although this indication will probably be more clear due to the increased magnitude of activity. The effectiveness of this test would not be diminished at these higher loads unless the minor damage inflicted by the higher loads and the microcracking would be of concern.

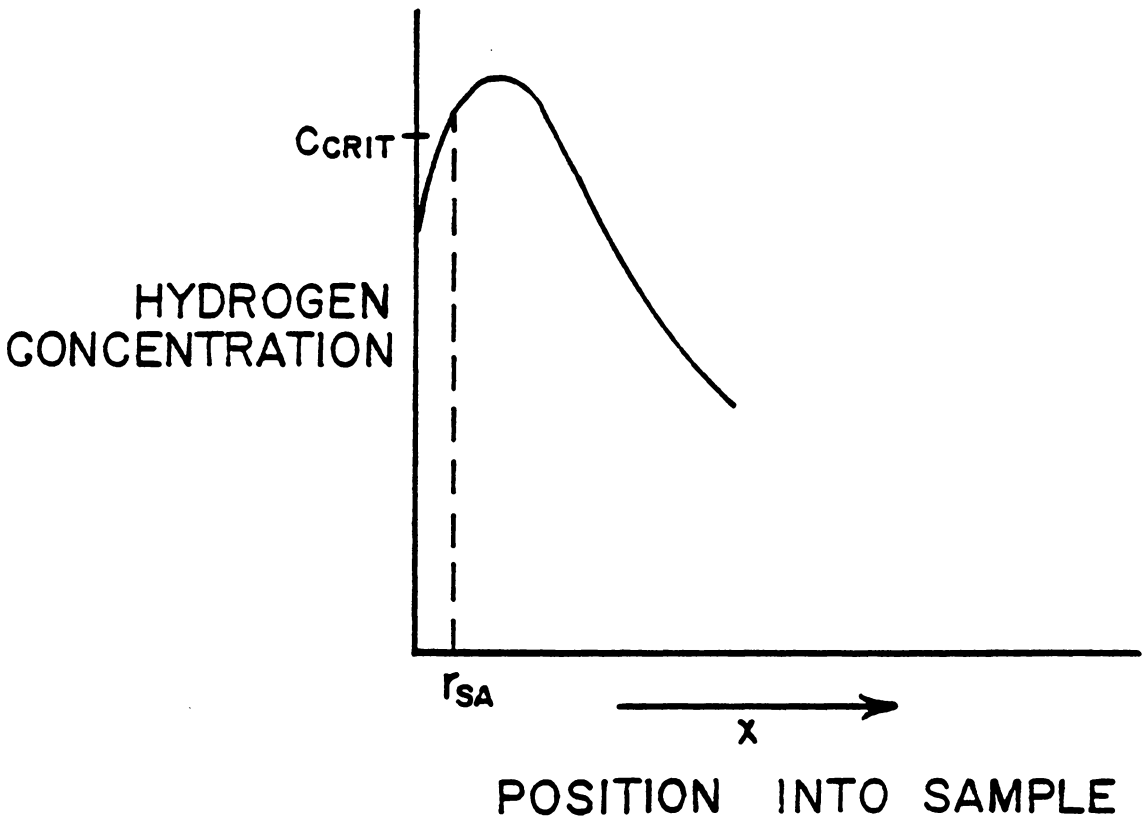

Figure 4.15. Schematic of near surface hydrogen concentration profile.

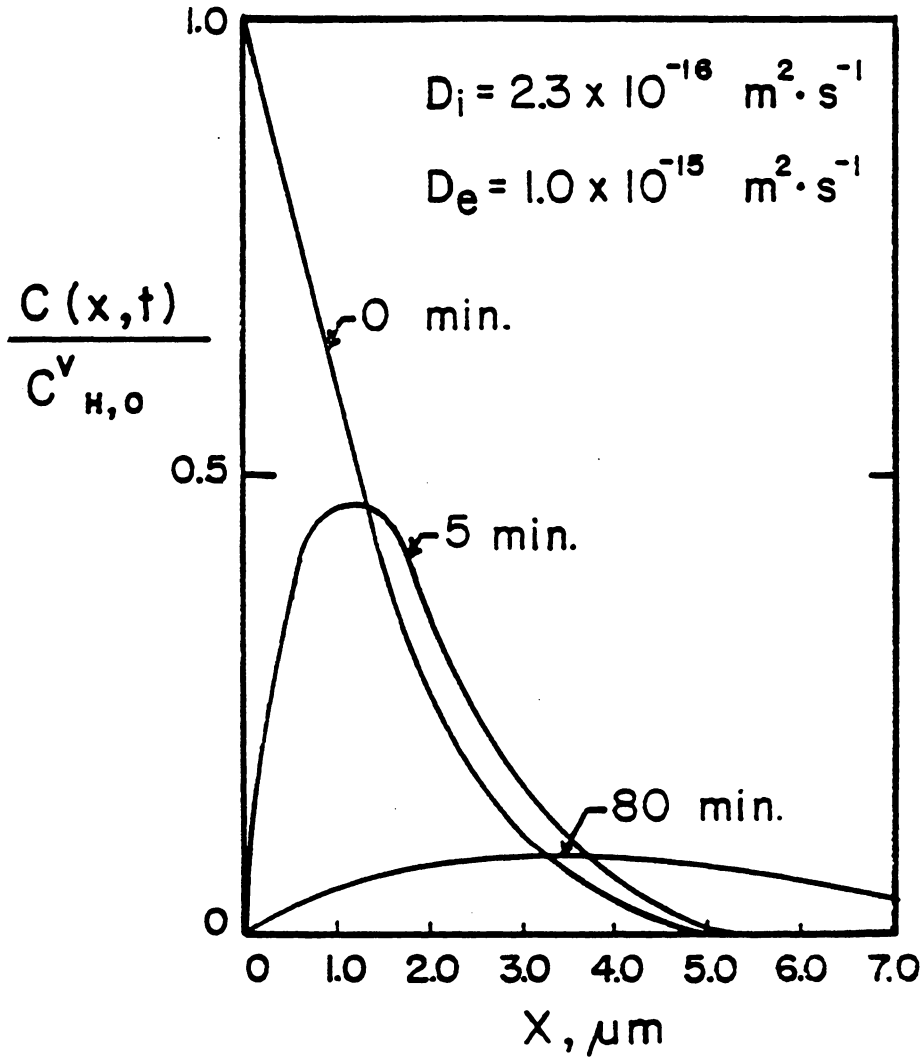

Figure 4.16. Computed concentration profile showing effects of near surface outgassing (after Coyle (73)). Di = ingress diffusivity, De = egress diffusivity.

4.4 *Pickling*

Pickling experiments were conducted to determine if small amounts of hydrogen adsorbed during a common industrial procedure could be detected. The data shown in Tables 4.5 and 4.6 reflect the large amount of data scatter that results from a lack of test repetition and averaging. The scatter was also enhanced by the build-up of an oxide film on the specimen surface. It is thought that in certain instances the fracture of the film upon indentation generated some activity. During the time necessary to prepare for testing after pickling (2 to 4 minutes) a large percentage of the adsorbed hydrogen had diffused from the specimen. This time was quite large in comparison with pickling times. If a specimen could have been tested within these first few minutes the level of activity probably would have been much higher.

Despite these problems, the drop in activity over time is clear. AE energy levels dropped to zero at a time roughly corresponding with pickling time. The surface was not altered in any way following the post-charge grinding and cleaning. Therefore, any decrease in activity could not be attributed to events related to film rupture. This decrease must then be related to hydrogen outgassing.

The ability of this test system to detect the effects of dilute HCl is of particular interest because of the frequency with which such a process is conducted in industry.

4.5 *Surface effects*

The surface finish results shown in Table 4.7. Indicate the strong dependence of AE activity on surface finish. The roughest surface finish showed the most dramatic post-charge activity and the

Table 4.5. AE Energy Per Indentation Versus Time of Test for Polished Pearlitic-Ferritic A-106B Steel Pickled for 10 Minutes in 10 Volume Percent HCl.

Time after Removal from Pickling Bath (minutes)	AE Energy Per Indentation (arbitrary units)
4:00	181
5:11	22
6:01	13
6:51	32
7:46	37
8:34	24
9:23	95
10:03	75
10:54	21
11:30	10
12:06	1
12:58	23
13:43	6
14:43	7
15:31	31
16:26	0
17:08	0
17:51	24
18:41	2
19:20	0
20:00	0
20:45	2
21:34	0
22:13	0
22:53	0

Table 4.6. AE Energy Per Indentation Versus Time of Test for 400 Grit Pearlitic-Ferritic A-106B Steel Pickled for 15 Minutes in 20 Volume Percent HCl.

Time after Removal from Pickling Bath (minutes)	AE Energy Per Indentation (arbitrary units)
1:20	6
2:27	2
2:58	2
3:35	25
4:13	2
4:43	0
6:17	20
7:03	0
7:45	0
8:28	63
10:00	17
10:48	10
11:23	5
11:59	6
13:05	0
14:30	12
15:10	0
15:49	0
16:24	0
17:01	0
17:42	0
18:25	0
19:10	0

Table 4.7. Effect of Surface Finish on Detected AE Energy.

Surface Finish	AE Energy
60 grit	236
320 grit	50
Chemical polish	30

most significant change in activity after charging. Previous findings have shown that hydrogen adsorption decreases with increased surface roughness (74). Therefore, it is possible that with less hydrogen present, more activity is generated in the 60 grit specimen. This phenomenon may be due to higher stresses being generated in the near surface region of the rougher sample. Other investigations have indicated greater hydrogen adsorption through rougher surfaces. If this is the case, the increased magnitude of activity is merely reflecting the higher hydrogen concentration (75). Discernment between these two effects could have been made by maintaining a consistent surface on a small area containing the indenter and transducer while varying roughness on the bulk of the sample.

This information suggests that, aside from cleaning, little surface preparation would be necessary before conducting an indentation test on a component. In fact, polishing may decrease the effectiveness of such a test. Because of the variation in activity due to surface roughness, care should be taken to maintain consistency in surface finish when comparing activity values from test to test.

In the course of investigating surface roughness effects, it was noted that AE energy levels of uncharged samples were high immediately after 60 grit wet grinding. These high levels decayed within a few minutes to consistent baseline readings. It is thought that small amounts of hydrogen may have been adsorbed during the wet grinding process and caused these increased activity levels. The detection of these small amounts of hydrogen at the very near surface of the specimen further indicates the sensitivity of this test procedure.

4.6 *Data Scatter*

The degree of data scatter has frequently been mentioned throughout this discussion. Clearly the effectiveness of this technique would be significantly enhanced if the degree of scatter could be reduced.

Data for a gaseous charging trial is shown again in Figure 4.17. In this figure, error bars which represent one standard deviation are provided to indicate the relative degree of scatter typical in the 10 individual tests which were conducted to generate one data point. This degree of scatter is typical of all of the tests conducted and clearly is very large.

Because the sources of the emission were near the surface of the test samples and surface waves are likely to have been propagated, it is thought that the surface effects are contributing to scatter more heavily than are source differences. The two predominant surface effects are likely to be the presence of surface discontinuities (deep scratches or cracks) between the indenter and transducer and inconsistencies in coupling the transducer to the surface. The major source scatter could possibly be identified by detecting the emission simultaneously at various points on the surface. The four channels of the AE detection system would facilitate this procedure. Therefore, any difference in the detected signal among the four transducers would be entirely due to differences in propagation of the AE energy in the material or to differences in coupling. Pinpointing this source of scatter surely would facilitate its reduction.

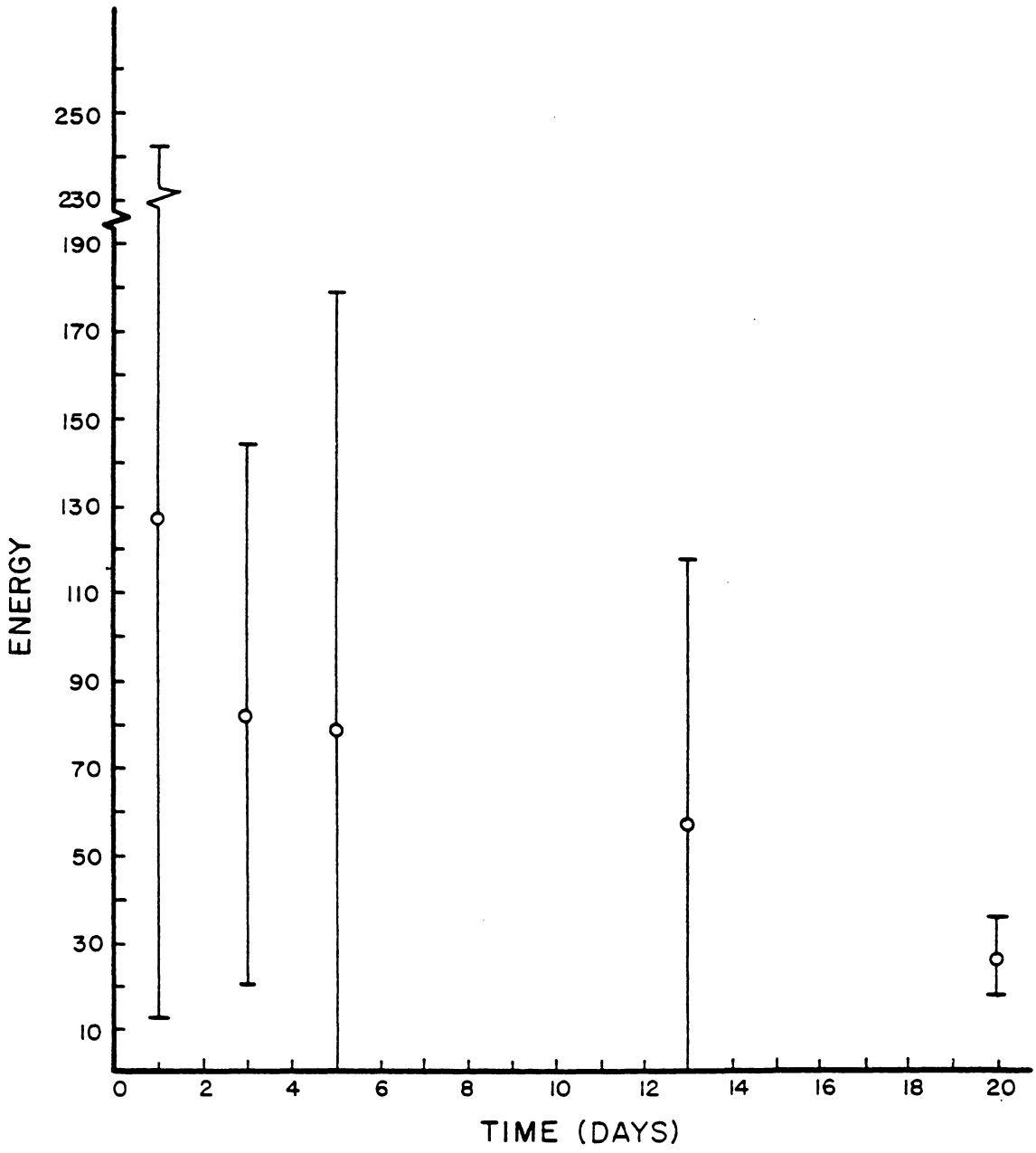

Figure 4.17. AE energy as a function of time for gaseous charging. Error bars representing one standard deviation.

4.7 *Implementation of the test procedure*

The most immediate application of the indentation test procedure is for monitoring adsorption during plating operations. During electroplating, hydrogen uptake will result from pickling which is done to prepare the surface of the base metal for electroplating and from the electrochemical process by which the plating material is applied. The effectiveness of the indentation technique in detecting hydrogen from both of these processes has been established. However, there are some points that need to be reiterated regarding the details of implementing this test procedure, some of which are relevant to the testing of any material for the presence of hydrogen and others which apply specifically to the monitoring of plating processes.

The first stage of implementing this procedure would be the determination of the hydrogen concentration at which the performance of the material would be degraded to a critical level. The level would have to be determined destructively based on the degradation of some relevant mechanical property or by noting a change in fracture mode of the component. The details of this determination are quite complex but critical hydrogen concentrations have been established for specific metals and alloys (76). These concentrations are very low and are very dependent on the metallurgical condition of the material. In order to avoid the complexity of determining the degree by which a given hydrogen concentration damages a metal or alloy, any AE energy level above that corresponding to a hydrogen free component may be termed critical. Although this level is conservative, it would be much easier to guarantee that no hydrogen degradation will occur if the hydrogen content is essentially zero than to guarantee that some predetermined content based on a specific level of activity would not affect performance. If a conservative estimate will not suffice, the AE energy level corresponding to the previously determined critical concentration must be found by testing a component in a specific metallurgical condition containing a specified hydrogen concentration. By whatever means this critical activity level is formulated, a large number of tests must be performed so that, despite data scatter, the acceptable AE energy level is clear. The AE

energy level is then used as an accept/reject criterion for the component of interest. Multiple tests and averaging must again be conducted on the component. If the average AE per indentation level of the component exceeds the predetermined accept/reject criterion the component can be removed from service or procedures can be implemented for removal of the hydrogen from the material. The AE activity level is a strong function of material, geometry, surface finish, indenter load and AE system parameters. Therefore, any minor change in these parameters may necessitate a reformulation of the critical AE energy level.

Monitoring a plating operation for hydrogen uptake requires some special considerations, because the plating material will be likely to possess very different mechanical and hydrogen transport properties than the base metal. Sufficient indenter loads must be used to insure that the stress field of the indentation extends through the plate to the base metal. The effectiveness of the indentation procedure in testing through a surface layer has been verified to an extent in the pickling experiment. In that experiment, the drastically different mechanical properties of the oxide film and A106 steel were not of consequence because fracture of the oxide was independent of hydrogen concentration in the base metal and therefore occurred at a constant level throughout all of the tests. Under these conditions, any emissions resulting from the plated surface layer due to mechanical differences from the base metal will remain constant. Therefore, as long as the indenter load penetrates through the surface layer and the thickness of this layer is uniform no obvious problems would result. However, because of the complex hydrogen distribution and the nonuniform mechanical properties of the component after plating, it is recommended that an outgassing profile be generated for the particular component which has been plated. This graph of AE energy versus bake-out time would reflect any difficulties that might arise from the tst procedure specific to that particular component. From this profile the critical activity level and also the bake-out time corresponding to that level could be determined. This bake-out time would be used on all of the plated components and the AE indentation test could then be employed on individual components as a control measure to verify the effectiveness of the indentation test and bake-out procedure. It therefore appears that there are no problems inherent to the test procedure that would prevent its

application to plated components in particular or, in general, to any material which has been exposed to hydrogen. Further investigations which are clearly necessary before this procedure can be implemented are suggested in the following section.

5.0 Conclusions and Recommendations

The results of this investigation show that the presence of hydrogen in a material can be detected by monitoring of acoustic emission from microhardness indentations in the material. Specifically:

1. Acoustic emission energy levels increased greatly following various means of hydrogen charging

2. These energy levels then decreased with time. This decrease was shown to be associated with diffusion controlled outgassing through the calculation of a hydrogen diffusivity based on the AE levels.

3. Factors such as surface condition, microstructure, instrumentation parameters, and indenter load have been shown to substantially affect the resulting AE activity levels.

4. AE generation appears to result from breakaway of dislocations from Cottrell-like hydrogen atmospheres.

This investigation favorably demonstrates the feasibility of implementing this technique as a non-destructive test to denote the presence of hydrogen in a material and in particular to evaluate effectiveness of bake-out procedures following electroplating. The following procedures are recommended for further development of this technique:

1. Applying the technique to plated components at various stages of bake-out.

2. Apply the technique to martensitic structures with high hydrogen concentrations (using high loads if necessary) to see if detectable cracking results.

3. Utilize the 4 channel capability of the AE system to investigate the effects of propagating media and surface discontinuities on AE levels by positioning four transducers simultaneously on the indented surface or by positioning the transducers on the opposing face of the sample.

4. Correlation of AE energy levels with some measure of hydrogen damage such as change in fracture mode.

References

1. Tetelman, A. S., Fundamental Aspects of Stress Corrosion Cracking, NACE, Houston, TX, 1969, p. 446.

2. Leeuwen, H.P., Engineering Fracture Mechanics, Vol. 6, p. 141, 1974.

3. Jenson, W. L., "Failures of Mechanical Fasteners," Failure Analysis and Prevention Handbook, 8th Edition, ASM, 1975.

4. Sudarshan, T. S., Louthan, M. R., Jr., McNitt, R. P., Scripta Met., Vol. 12, 1978, p. 799.

5. Cialone, H., Asaro, R. J., Met. Trans., Vol. 10A, March, 1979, p. 367.

6. Nelson, H. G., Effects of Hydrogen on Behavior of Materials, A. W. Thompson and I. M. Bernstein, eds., AIME, N.Y., 1976, p. 602.

7. Walters, R. J., et al., Effects of Hydrogen Behavior of Materials, A. W. Thompson, I. M. Bernstein, eds., AIME, N.Y., 1976, p. 273-298.

8. Louthan, M. R., Jr., McNitt, R. P., Proceedings of DOE Energy Storage and Hydrogen Energy Systems, Nov. 1977.

9. Sridhar, N., McNitt, R. P., Louthan, M. R., Jr., Recent Advances in Engineering Science, p. 1037, 1977.

10. Louthan, M. R., Jr., McNitt, R. P., Sridhar, N., Environmental Degradation of Engineering Materials, M. R. Louthan and R. P. McNitt, eds., VPI & SU, 1977.

11. Louthan, M. R., Jr., Caskey, G. R., Int. J. of Hydrogen Energy, Vol. 1, p. 291, 1976.

12. Bernstein, I. M., Thompson, A. W., Hydrogen Effects in Metals, AIME, NY, p. 291.

13. Coyle, R. J., et al., Environmental-Sensitive Fracture of Engineering Materials, edited by Z. A. Foroulis, 1977, p. 435.

14. Cornet, M., Talbot-Besnard S.

15. Louthan, M. R., Jr., Caskey, G. R., Donovan, J. A., Rawl, D. E., Jr., Materials Science and Engineering, Vol. 10, p. 289 (1972).

16. Hancock, C. G., Johnson, H. H., Trans. AIME, Vol. 236, p. 513, 1966.

17. Adler, T. A., Ph.D. Dissertation, VPI & SU, 1980.

18. Oriani, R. A., Stress Corrosion Cracking and Hydrogen Embrittlement of Iron Base Alloys, NACE, Houston, TX, 1977, p. 351.

19. Pussegodi, L. N., Tyson, W. R., Hydrogen Effects in Metals, AIME, NY, 1980, pg. 349.

20. Oriani, R. A., Josephic, R. H., Met. Trans., Vol. 11A, 1980, p. 1809.

21. Swearengen, J. C., Greulich, F. A., Liplain J., Environmental Degradation of Engineering Materials, VPI & SU, 1981, p. 303.

22. Lynch, S. P., Hydrogen Effects in Metals, AIME, NY, 1980.

23. Beachem, C. D., Met. Trans., Vol. 3, Feb., 1972, p. 437.

24. Louthan, M. R., Jr., McNitt, R. P., Effect of Hydrogen on Behavior of Materials, AIME, NY, 1976, p. 496.

25. Louthan, M. R., Jr., McNitt, R. P., Murali, J., Sridhar, N., Sudarshan, T. S., Hydrogen Energy Systems, Vol. 4, p. 2503.

26. Troiano, A. R., Trans ASM, 1960, Vol. 52, p. 54.

27. Louthan, M. R., Jr., Derrick, R. G., Donovan, J. A., Caskey, G. R., Effect of Hydrogen on the Behavior of Materials, AIME, NY, 1976.

28. Louthan, M. R., Jr., McNitt, R. P., Advances in Engineering Science, SESA NASA CP 2001, Vol. 1, p. 77, 1976.

29. Sudarshan, T. S., Louthan, M. R., Jr., McNitt, R. P., Scripta Met., Vol. 12, 1978, p. 799.

30. Louthan, M. R., Jr., McNitt, R. P., Murali, J., Sudarshan, T. S., Adler, T. A., Proc. of DOE Chemical/Hydrogen Energy Systems Conference, p. 351, 1979.

31. West, A. J., Louthan, M. R., Jr., Met. Trans., Vol. 10A, p. 1675, 1979.

32. Sisson, R. D., Jr., Adler, T. A., Wilson, J. H., Louthan, M. R., Jr., Scripta Metallurgica, Vol. 14, 1980, p. 1207.

33. Adler, T. A., Louthan, M. R., Jr., McNitt, R. P., Microstructural Science, Vol. 8, 1980, p. 217.

34. Lewis, B. A., Louthan, M. R., Jr., Wagner, J., Sisson, R. D., McNitt, R. P., Louthan, M. R., III, Proceedings of Miami International Symposium on Metal Hydrogen Systems, Edited by T. Negat Veziroglin, 1982.

35. Louthan, M. R., Jr., Caskey, G. R., Donovan, J. A., Microstructural Science, Vol. 3, p. 823, 1975.

36. Blackmore, J. S., Met. Trans., 1, 145, 1970.

37. Oriani, R. A., Environmental Degradation of Engineering Materials in Hydrogen, VPI & SU, 1981, p. 3.

38. Gibala, R., Stress Corrosion Cracking and Hydrogen Embrittlement of Iron Based Alloys, NACE, 1977, p. 244.

39. Miodownik, A. P., Stress Corrosion Cracking and Hydrogen Embrittlement of Iron Based Alloys, NACE, 1977, p. 274.

40. Barth, C. F., Steigerwald, E. A., Met. Trans., Vol. 1, Dec. 1970, p. 3451.

41. Beachem, C. D., Stress Corrosion Cracking and Hydrogen Embrittlement at Iron Based Alloys, NACE, 1977, p. 376.

42. Gerberich, W. W., Hartbower, C. E., Fundamental Aspects of Stress Corrosion Cracking, NACE, Houston, TX, 1969.

43. Tien, J. K., Effect of Hydrogen on Behavior of Materials, Thompson and Bernstein, eds., 1975, AIME, p. 309.

44. Liptai, R. G., Harris, D. O., Tatro, C. A., ASTM STP 505, ASTM, 1972, p. 3.

45. Spanner, J. C., Acoustic Emission Techniques and Application, Intex, Evanston, IL, 1974.

46. Frank, R. C., Internal Stresses and Fatigue in Metals, Elsevier Press, 1979.

47. Ono, K., Stern, R., Lang, M., ASTM STP 505, 1972, p. 152.

48. Fowler, K. A., Papandakis, E. P., ASTM STP 505, ASTM 1972, p. 222.

49. Dunegan, H. L., Green, A. I., Materials Research and Standards, Vol. II, p. 21, Mar, 1971.

50. Kudryavtsev, V. N., Schmitt-Thomas, Kh.G., Stengel, W., Waterschek, R., Corrosion, Vol. 37, No. 12, Dec., 1981.

51. Heiple, C. R., Carpenter, S. H., Carr, M. J., Metal Science, Vol. 15, Nov./Dec., 1981, p. 587.

52. Clough, R. B., Wadley, H. N. G., Met. Trans., Vol. 13A, Nov., 1982, p. 1965.

53. Clough, R. B., Simmons, J. A., Materials Evaluation, October, 1981, p. 1027.

54. Lawn, B. R., Fuller, E. R., J. Matls. Sc., 1975, Vol. 10, p. 2016.

55. Hadjicostis, A. N., Carpenter, S. H., Materials Evaluation, Feb. 1980, p. 19.

56. Tetelman, A. S., Chow, R., ASTM STP 505, ASTM 1972, p. 30.

57. Vol. 11, ASM Metals Handbook, pg. 1, ASM, 1976.

58. Samuels, Le, ASTM STP 889, ASTM, p. 5.

59. Hirst, W., Howse, M. G. J. W., Proc. R. Soc. London, Ser. A, 311, 1969, p. 429.

60. Perrott, Wear, 45 (1977) p. 293.

61. Evans, A. G., Charles, E. A., J. Am. Ceram. Soc., 59 [7-8] 371-372 (1976).

62. Lawn, B. R., Fuller, E. R., Journal of Materials Science, Vol. 19, 1984, p. 4061.

63. Lawn, B. R., Wilshaw, R., Journal of Materiasl Science, Vol. 10 (1975) p. 1049.

64. Miller, M., Physical Acoustics Technical Representative, personal conversation regarding work in progress.

65. Donovan, J. A., Met. Trans., Vol. 7A, Jan., 1976, p. 145.

66. Crank, Mathematics of Diffusion, 2nd Edition, Clarendon Press Oxford, 1975.

67. Krautkramer, J., Krautkramer, H., Ultrasonic Testing of Materials, Springer-Verlag, Berlin/Heidelberg, p. 89 (1969).

68. Clough, R. B., Chang, J. C., Travis, J. P., Scripta Met., Vol. 15, p. 417.

69. Murali, J., Ph.D. Dissertation, VPI & SU, 1980.

70. Reed-Hill, R. E., Physical Metallurgy Principles, Wadsworth, Inc., Monterray, Cal., 1973, p. 338.

71. Gillis, PP, ASTM STP 505, ASTM 1972, p. 20.

72. James, D. R., Carpenter, S. H., Journal of Applied Physics, Vol. 42, No. 12, Nov. 1971, p. 4685-4697.

73. Coyle, R. J., Atrens, A., Fiore, N. F., Bellina, J. J., Jolles, M., Environment-Sensitive Fracture of Engineering Materials, Forovlis, Z. A., ed., AIME, 1979, p. 431.

74. Louthan, M. R., Jr., Predictive Capabilities in Environmentally Assisted Cracking, ed. by R. Ruda, PVD, Vol. 99, p. 235, ASME (1985).

75. Louthan, M. R., Jr., Derrick, R. C., Corrosion Science, Vol. 15, p. 565 (1975).

76. Pressouyre, G. M., Current Solutions to Hydrogen Problems in Steels, ASM, Metals Park, OH, 1982, p. 18.

77. Fiore, N. F., Lunarska, E., Zielinski, A., Advanced Techniques for Characterizing Hydrogen in Metals, Fiore, N. F., Berkowitz, T. J., ed. AIME, NY, 1982, p. 189.

Appendix A. Description of Test System

The two major components of the test system are a Leco Model DM400 microhardness tester and a Physical Acoustics Corporation (PAC) 3000/3104 acoustic emission detection and analysis system. A photograph and schematic illustration of the test system are shown in Figures A1 and A2.

The desirable feature of the microhardness tester is the ability to deliver a highly reproducible, and localized load. This load is delivered by a Vicker's indenter and can range from 10g to 1Kg. The load can be applied for up to 30 seconds. This investigation used 1Kg loads for a duration of 10 to 15 seconds.

Acoustic emission resulting from the indentation process was detected with a PAC 150 KHz piezoelectric transducer. This transducer was positioned 1/2 inch from the source during the indentation tests on A106 and 4340 steels and 2 inches from the indenter during tests involving glass fracture. The transducer was coupled to the test sample with a thin layer of viscous PAC petroleum jelly conplant.

Following capture by the transducer, the signal is preamplified 40 dB using a PAC 1220A Acoustic Emission Preamplifier before reaching the 3000/3104 system. The physical and electrical specifications of the preamplifier and 3000/3104 system are described later in Appendix A. The 3000/3104 system provides addition variable amplification capabilities as well as extensive software for data analysis. The user friendly system has menu driven software which allows for manipulation and plotting of many AE parameters including amplitude, rise time, duration, energy, counts and frequency. The details and instructions for use of this software are described in detail in the PAC 3000/3104 User's Manual.

SPECIFICATIONS OF 1220 SERIES PREAMPLIFIERS

Electrical

Gain: 40 or 60 dB (Switch selectable)

Bandpass: User selectable from 10 KHz to 2.0 MHz

Input: Single or differential selectable

Input Impedance: 10KΩ 15 pF

Output Voltage: 20Vpp into 50

Dynamic Range: 90dB

CMRR (500KHz): 55dB

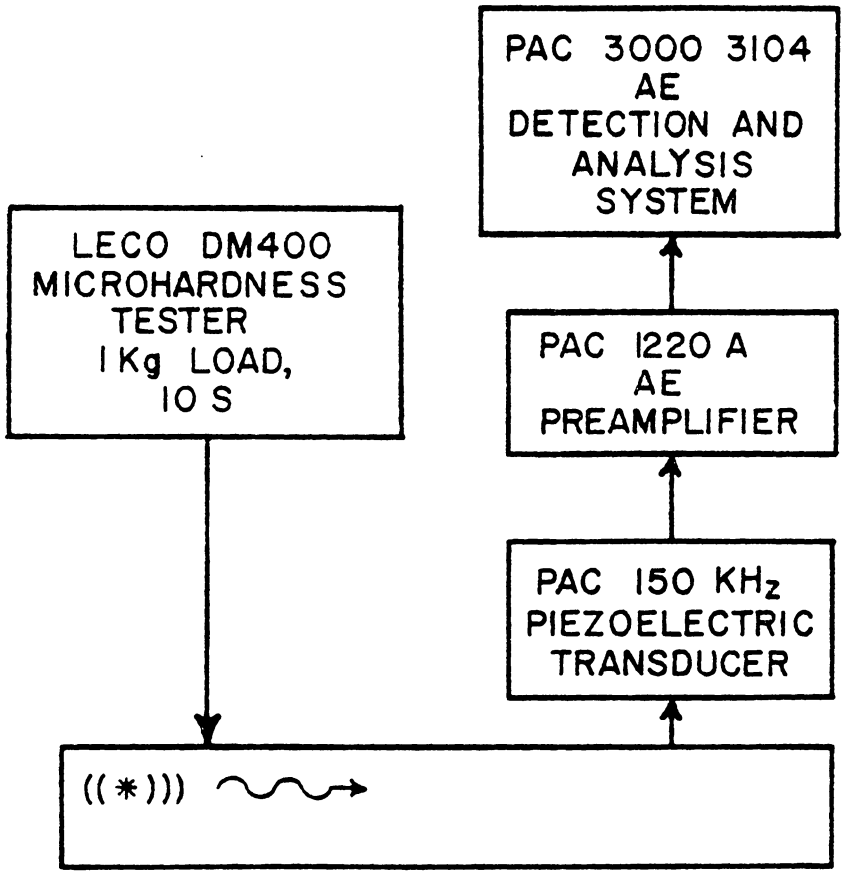

Figure A.1. Schematic of AE/Indentation Test System.

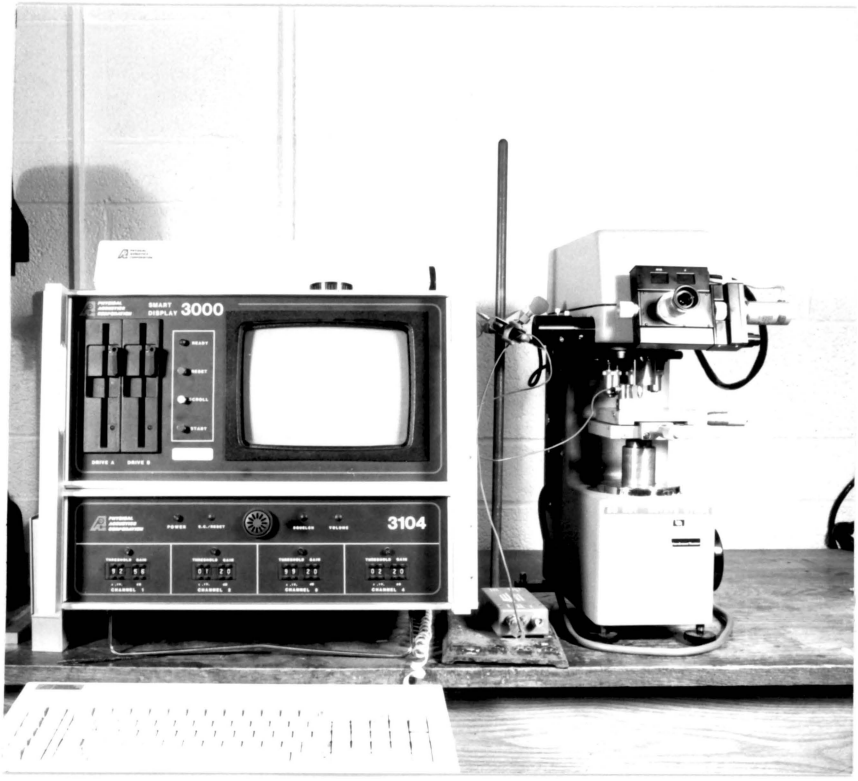

Figure A.2. Photograph of Test System.

Noise (RMS RTI): < 2μV

Power Requirements: 1220A,C- + 28VDC; 1220B- ± 15VDC

DC Standby Current: 25mA

DC Current at full output: 200 mA

Environmental

Specifications apply at 25°C + 5°C

Instrument will operate from 0°C to 50°C

Physical

Dimensions: 3cm x 6 cm x 11 cm

Weight: 0.25 Kg

PHYSICAL AND ELECTRICAL SPECIFICATIONS OF 3000/3104 SYSTEM

Physical

Height: 5.25 inches

Width: 19 inches

Depth: 21 inches

Weight: 25 lbs.

Electrical

High Frequency Analog Portion of 3400

Four identical channels capable of providing the following data set to the computer for storage and processing:

1. Δt measurements/channel
2. AE Counts/channel
3. AE Energy/channel
4. AE Event Duration/channel
5. Rise Time/channel
6. AE Burst Peak Amplitude/channel

A. AE Amplifiers

Noise: 4.5 μV RMS RTI @ 1 MHz BW and 50Ω R

Gain: 0-41 db, 16 front panel selections

Bandwith: 10 KHz - 1.2 MHz @ 3 db points

AE Out: 0-10 VAC into 50Ωand470 pf

AE IN: 10μV-10VAC

AE Input Impedance: 50Ω@ 120 pf

AE Filtering: 100-300 KHz Bandpass Filter via Plug-in Module

AE Threshold: .1-8V, 16 front panel selections

AE Level: 0-15V into 50Ω and 470 pf

AE Peak Amplitude: 0-10V

B. Miscellaneous Analog

Load Cell Monitor: 0-1V or 0-10 V (internal hardware change)

Preamp Power: 28 Volts, 100 m amp max.

Peak Detector Droop Rate: 5mv/ms.

C. Digital Section

t Counter Capacity: 20 Bits (2^{20} - 1 capacity)

t Resolution: 200 nanoseconds

Energy Count Capacity: 16 Bits (2^{16} - 1 capacity)

Event Duration Counter Capacity: 16 Bits

Event Duration Resolution: 10 microseconds

AE Count Capacity: 16 Bits

Rise Time Counter Capacity: 16 Bits

Rise Time Counter Resolution: 500 nanoseconds

Peak Amplitude Resolution: 10 Bits (A/D), 10 millivolt resolution

External Parameter Resolution: 10 Bits (A/D)

System Time Out: Variable via Program -- from 40μsec-3 minutes

Appendix B. Definition of AE Terminology

B.1. The following are general definitions for common AE terminology established by the ASTM Acoustic Emission Working Group, 1972.

1. Acoustic emission - Acoustic emission is the transient elastic wave generated by the sudden release of strain energy in a material.

2. Burst emission - qualitative description of emission signal with high amplitude, short duration, short rise time, and high energy. Typically associated with cracking and brittle behavior. Has appearance of rapidly decaying spike.

3. Continuous emission - qualitative description of emission signal with low amplitude, long duration, long-rise time and low energy. Typically associated with ductile processes and other low energy emission sources. Has appearance much like noise.

4. Emission event - rapid physical change in a material that releases energy, PAC establishes an individual "event" based on system parameters discussed in B.3.

B.2. A.E. Event Parameters - The PAC data acquisition software has established five event parameters for qualitative characterization of acoustic emission events. They are amplitude, energy, duration, rise time and counts. These events can be plotted independently by the system against time, per event and against each other for source characterization purposes. Figure B.1 illustrates the meaning of these parameters and they are defined as follows.

1. amplitude - voltage response of transducer due to excitation by the emission pulse.

2. event envelope - curve connecting points of maximum amplitude.

3. energy - area under event envelope calculated in the PAC system by software integration of area under event envelope.

4. duration - period of time in which the oscillating amplitude exceeds the threshold level.

5. rise time - period of time from when pulse crosses threshold until maximum amplitude is achieved.

6. counts - number of individual instances in which amplitude exceeds the threshold during an event.

B.3. The following are system parameters, set by the user. System parameters have a great effect on the AE parameters discussed in B.2, and therefore are critical to the system operation.

1. Threshold - (effective threshold) minimum amplitude which can be detected by the system, low threshold means more events of longer duration, more counts and higher energies will be detected. Effective threshold is related to the set threshold and gain by the following relationship

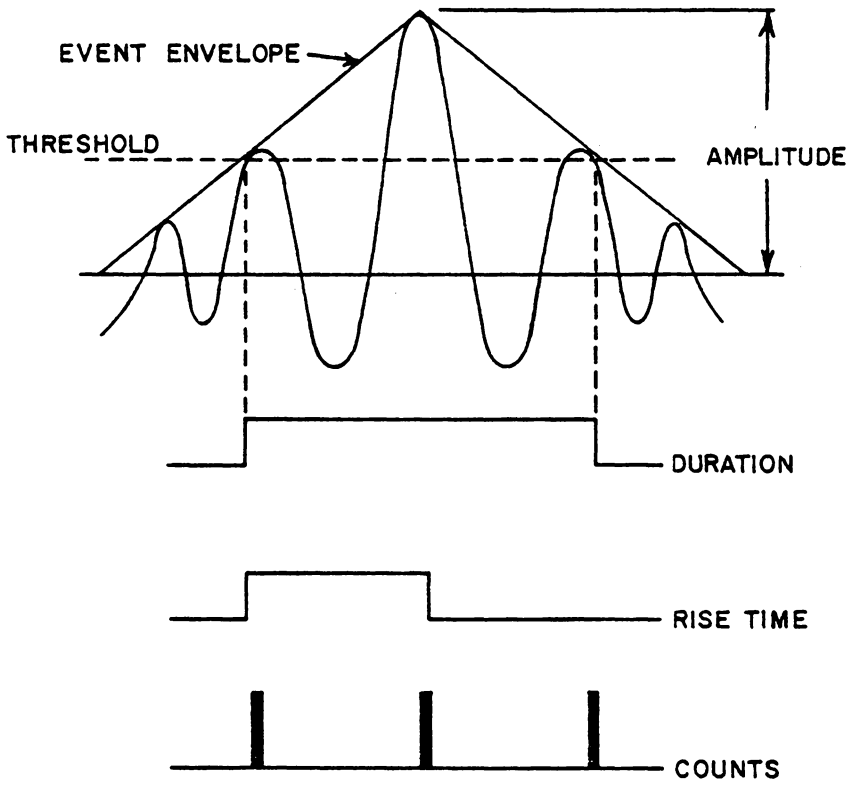

Figure B.1. Illustration of AE Parameters.

$$T_{eff} = 20 \log \frac{T_{set}\ (Volts)}{10^{-4}\ Volts} - GAIN$$

2. Dead Time - minimum period of time between events, signal must remain below threshold level for a period of time equal to the dead time in order for AE activity to be registered as two discrete events. Event envelope (Figure B.l) is constructed based on the value selected for dead time. Short dead time implies that AE activity will be broken into a series of small events with shorter duration fewer counts and less energy. Therefore, the effect of dead time on event parameters is significant.

3. Time Base - minimum time resolution of the system in terms of time at which an event occurs. Time base ranges from .0ls to 90s for the 3000/3104 system.

The vita has been removed from the scanned document